eNeuro

Research Article: New Research | Novel Tools and Methods

Graph theoretic and motif analyses of the hippocampal neuron type potential connectome

Abbreviated Title: Analysis of Hippocampome.org neuron type circuitry

Cl Rees, Dw Wheeler, Dj Hamilton, Cm White, Ao Komendantov and Ga Ascoli

Krasnow Institute for Advanced Study, George Mason University, Fairfax, Virginia 22030

DOI: 10.1523/ENEURO.0205-16.2016

Received: 13 July 2016

Revised: 21 October 2016

Accepted: 25 October 2016

Published: 7 November 2016

Author Contributions: CR designed research, performed research, analyzed data, and wrote the paper; DW performed research and analyzed data; DH contributed unpublished analytic tools; CW performed research; AK analyzed data; GA designed research, analyzed data, and wrote the paper.

Funding: NINDS (NIH)
R01NS39600

Funding: NSF
IIS-1302256

Funding: MURI (ONR)
N00014-10-1-0198

Funding: CENTEC (AFOSR)

Conflict of Interest: Authors report no conflict of interest.

This project was supported by grants NINDS R01NS39600 (NIH), NSF IIS-1302256, MURI N00014-10-1-0198 (ONR), and CENTEC (AFOSR). *Publication of this article was funded in part by the George Mason University Libraries Open Access Publishing Fund.*

Correspondence should be addressed to: Giorgio A Ascoli, ascoli@gmu.edu

Cite as: eNeuro 2016; 10.1523/ENEURO.0205-16.2016

1. **Manuscript Title**: Graph theoretic and motif analyses of the hippocampal neuron type potential connectome

2. **Abbreviated Title**: Analysis of Hippocampome.org neuron type circuitry

3. **List of All Author Names and Affiliations**:

Rees CL[1], Wheeler DW[1], Hamilton DJ[1], White CM[1], Komendantov AO[1], Ascoli GA[1]

[1]Krasnow Institute for Advanced Study, George Mason University, Fairfax, Virginia 22030

4. **Author Contributions**: CR designed research, performed research, analyzed data, and wrote the paper; DW performed research and analyzed data; DH contributed unpublished analytic tools; CW performed research; AK analyzed data; GA designed research, analyzed data, and wrote the paper.

5. **Correspondence should be addressed to:** Giorgio A Ascoli (ascoli@gmu.edu)

6. **Number of Figures**: 10
7. **Number of Tables**: 2
8. **Number of Multimedia**: 0
9. **Number of words for Abstract**: 205
10. **Number of words for Significance Statement**: 120
11. **Number of words for Introduction**: 444
12. **Number of words for Discussion**: 2063

13. **Acknowledgements**: We wish to thank Ben Holmes, Sean Mackesey, Keivan Moradi, and Siva Venkadesh for their help and insight.

14. **Conflict of Interest**: Authors report no conflict of interest

15. **Funding Sources**: This project was supported by grants NINDS R01NS39600 (NIH), NSF IIS-1302256, MURI N00014-10-1-0198 (ONR), and CENTEC (AFOSR). Publication of this article was funded in part by the George Mason University Libraries Open Access Publishing Fund.

Abstract

We computed the potential connectivity map of all known neuron types in the rodent hippocampal formation by supplementing scantly available synaptic data with spatial distributions of axons and dendrites from the open-access knowledge base Hippocampome.org. The network that results from this endeavor, the broadest and most complete for a mammalian cortical region at the neuron-type level to date, contains more than 3,200 connections among 122 neuron types across six sub-regions. Analyses of these data employing graph theory metrics unveil the fundamental architectural principles of the hippocampal circuit. Globally, we identify a highly specialized topology minimizing communication cost; a modular structure underscoring the prominence of the tri-synaptic loop; a core set of neuron types serving as information processing hubs as well as a distinct group of particular anti-hub neurons; a nested, two-tier rich club managing much of the network traffic; and an innate resilience to random perturbations. At the local level, we uncover the basic building blocks, or connectivity patterns, that combine to produce complex global functionality, and we benchmark their utilization in the circuit relative to random networks. Taken together, these results provide a comprehensive connectivity profile of the hippocampus, yielding novel insights on its functional operations at the computationally crucial level of neuron types.

Significance Statement

Brain connectomes are being constructed at two disjointed levels. Microscopically, the wiring of individual neurons is being accumulated into cumbersome synaptomes; macroscopically, region-to-region projectomes obscure important circuit details. Neuron types provide a fertile middle ground. Using the 122 hippocampal formation types from Hippocampome.org, we augmented sparse connectivity knowledge with morphological evidence to obtain a full “potential connectome.” Though this network contains >3,200 connections that are not easily amenable to intuitive hypothesis generation and testing, such complexity can be tackled using graph theory analysis, whereby we

47 investigate the relationship between the circuit's connectivity properties and functions. As type-level
48 data grows, the array of analyses detailed here can be extended to rapidly supplement our
49 understanding of the computational operation of the hippocampus.

50

51 **Introduction**

52 The rodent hippocampus encompasses millions of neurons (West et al., 1991; Hosseini-Sharifabad
53 and Nyengaard, 2007; Bandeira et al., 2009; Fu et al., 2013), each synapsing with tens of thousands
54 of others (Gulyás et al., 1999; Megías et al., 2001). Examination and quantitative analysis of
55 anatomical connectivity constitute a critical step towards understanding the circuit function (Sporns et
56 al., 2005).

57 Major community efforts like the BRAIN Initiative (Insel et al., 2013) and the Human Brain Project
58 (Markram et al., 2015) are currently attempting to reconstruct the entire synaptic connectivity of each
59 individual neuron. These undertakings produce massive datasets, but their necessary focus on
60 extremely contained anatomical domains cannot comprehensively reveal long-range circuit
61 architecture (see e.g. Mishchenko et al., 2010; Kasthuri et al., 2015). At the other extreme,
62 approaches such as the Human Connectome Project (van Essen et al., 2013) and the Allen Mouse
63 Brain Connectivity Atlas (Oh et al., 2014) use diffusion tensor imaging or anterograde/retrograde
64 tractography to map brain-wide regional connectivity (see also Mitra, 2014; Zingg et al., 2014).
65 However, the limited spatial resolution and lack of cellular specificity restrict the utility of these data to
66 inform our understanding of neuronal computation.

67 In between these popular "synaptome" (DeFelipe, 2010) and "projectome" (Kasthuri and Lichtman,
68 2007) levels lies an arguably more immediately fertile neuron-type circuitry approach that intuitively
69 harmonizes well with Cajal's "Neuron Doctrine" (Shepherd, 1991). Though neurons are indeed unique
70 cellular units, they may be readily grouped according to sets of properties that cluster along a
71 continuum. Over the past six years, we mounted a massive literature search to catalog all known

neuron types in the rodent hippocampal formation based on their main neurotransmitter, axonal-dendritic morphologies, somatic location, molecular expression, and electrophysiological parameters (Wheeler et al., 2015). All the properties (and underlying experimental evidence) of the resulting 122 neuron types are collated in a publicly available, highly curated knowledge base (Hippocampome.org) that is ripe for analysis along multiple dimensions.

Here, because knowledge about synaptic connectivity among the types is sparse, we fill the gaps by exploiting Peters' rule (Braitenberg and Schüz, 1991), which recognizes axon-dendrite juxtapositions among the types as potential connections. We then quantitatively examine the resulting complex network using graph theory (Bullmore and Sporns, 2009; Rubinov and Sporns, 2010; Wig et al., 2011; Binicewicz et al., 2015). Through a suite of analyses, we investigate global degree distribution, circuit modularity, rich club coefficients, absorption and driftness, as well as local motif composition, in order to foster intuition on how the functionality of the hippocampus relates to its fundamental architectural properties (Sporns et al., 2000). We also present an interactive, online, open-source toolbox for exploring the potential neuron-type connectome in the rodent hippocampal formation.

Materials and Methods

Identification of neuron types

This work focuses on the rodent (mouse and rat, of either sex) hippocampal formation, defined as the dentate gyrus (DG), CA3, CA2, CA1, subiculum, and entorhinal cortex (EC). Each of these sub-regions is divided in layers (e.g. CA3 oriens, pyramidale, lucidum, radiatum, and lacunosum-moleculare; or EC L1-L6) giving rise to a total of 26 anatomical parcels. Over a period of several years, we amassed information on hippocampal formation neuron types from the century-deep and information-rich body of literature. However, because neurons are often named on an *ad hoc* basis without full mappings to previous names and descriptors (Hamilton et al., 2016), author-provided names of types were treated warily. Instead, neuron types were identified chiefly based on their

primary neurotransmitter (i.e. glutamate or GABA) and for having a unique binary pattern of axonal and dendritic presence or absence across the 26 parcels (see Wheeler et al., 2015 for details). In rare cases (e.g. fast-spiking/parvalbumin-positive and regular-spiking/cholecystokinin-positive basket cells, or ivy and bistratified cells), aligned molecular marker and electrophysiological evidence was sufficiently different to support the creation of two distinct types out of neurons with the same morphological pattern and primary neurotransmitter. Type names were then selected, differentiated, combined, or created anew in order to minimize confusion with the existing literature and fully mapped to their synonyms (see Hamilton et al., 2016 for explanation). The complete set of terms, definitions, data, and supporting experimental evidence collectively underlying the identification of the resulting 122 hippocampal neuron types is publicly available in open access form at Hippocampome.org (RRID: SCR_009023). Table 1 provides a glossary of neuron types to facilitate identification in figures throughout the paper.

Culling of known connectivity information

All 484 peer-reviewed literature references comprising v1.0 of the Hippocampome.org knowledge base were mined in a first-pass attempt to determine which of the 14,884 (122^2) directed pairs of neuron types are known to synapse, or known not to synapse. Information verified by various methods (e.g. electron microscopy or electrophysiological paired recordings) was annotated and relevant quotes and figures were extracted. Future versions of Hippocampome.org will additionally examine sources that cite and those that are cited by the original references, as well as search for specific peer-reviewed articles with neuron-type connectivity information.

Computation of potential connectivity

In the absence of literature evidence for known connections or non-connections, information on potential connectivity between types was exploited in order to achieve a full hippocampal connectome

(simply referred to as HC in the remainder of the paper). The co-existence of the axons of one type with the dendrites of another within any hippocampal formation parcel indicates relative spatial proximity and a potential for synapsing. The rows in Figure 1A show a subset of neuron types and their defining axo-dendritic patterns. For example, the axons of Granule cells are present in the DG hilus (H), CA3 stratum lucidum (SL) and stratum pyramidale (SP), and CA2 SP. Therefore, any neuron type with dendrites in any one or more of these parcels, including Mossy-Fiber-Associated Oriens-Dendrite (MFA ORDEN) cells (type 37 in Table 1), is a potential target of the Granule cell axons (Fig. 1B). Further, types that do not have dendrites in the aforementioned parcels are excluded as potential Granule cell targets because of the lack of neurite overlap. This approach was extended to account for axo-somatic and axo-axonic connections of basket and chandelier cells, respectively. Mathematically, 26-dimensional binary vectors were utilized to encode the presence or absence across hippocampal parcels of the axon of each potential pre-synaptic type and of the dendrites (or soma or axonal initial segment) of each potential post-synaptic type. Potential connectivity was then calculated as the dot-product of these vectors: a non-zero result indicated a potential connection whereas a zero-value dot-product denoted that connectivity was not possible between the types in question.

$$\text{Axons of type } \vec{\mathrm{A}} = \langle a_1, a_2, \ldots, a_{26} \rangle$$

$$\text{Dendrites of type } \vec{\mathrm{D}} = \langle d_1, d_2, \ldots, d_{26} \rangle$$

$$c = \vec{A} \cdot \vec{D}$$

Many neuron types (101/122, not including Granule cells) have axons and dendrites co-located within one or more parcels, indicating the potential for within-type connectivity; such self-connections are not necessarily indications of single-neuron autapses.

A web-accessible resource for connectome visualization

A Java-based online toolbox was developed and deployed (Hippocampome.org/connectivity; click "Launch" button or link to "Potential Connectivity Map") to assist in the visualization and exploration of the HC. Glutamatergic (excitatory) and GABAergic (inhibitory) neuron types are represented as black and gray circles, respectively, and are placed randomly within the parcel (or along the parcel boundary) where their soma is most commonly located. Hovering over a type reveals its name; clicking on a type displays all of the connections that may be received by its dendrites (lines with arrows in) or sent by its axons (arrows out). A snapshot of the toolbox, taken after the selection of Granule cells, is shown in Fig. 1C. Toggles provide the ability to show or hide additional information, including connections made by the other (i.e. unselected) types and schematic illustrations of many of the major cell types and pathways in the hippocampal circuit.

Graph theory analyses

The Brain Connectivity Toolbox (BCT: Rubinov and Sporns, 2010; brain-connectivity-toolbox.net) was utilized to compute many graph theory measures for the HC. In certain cases, the MATLAB code was modified slightly to allow (or correct) for the possibility of self-connections of neuron types along the main diagonal of the connectivity matrix. In addition, some topological metrics were measured on the unweighted network while others mandated connections weighted by the sign of the primary neurotransmitter of the pre-synaptic type: +1 for glutamatergic and -1 for GABAergic. To study the robustness of our results, we also examined a version of the network wherein connections of the most numerous principal cell (PC) types, namely DG Granule cells, CA3 Pyramidal cells, and CA1 Pyramidal cells, were weighted as +10.

Clustering coefficient, characteristic path length, and degree

Certain standard measures, including clustering coefficient (CC) and characteristic path length (CPL),

are used to encapsulate the topology of the graph and are thus computed on a static, binary version of the network that disregards excitation and inhibition. Briefly, clustering coefficient is the fraction of connections among the immediate neighbors of a node (i.e. the set of neuron types that may receive information directly from that node) relative to the number of possible connections (Fagiolo, 2007). For example, Granule cells have 33 immediate neighbors that are interconnected with 476 (out of a possible 33^2=1089) edges; $CC_{Granule}$ = 476/1,089 = 0.437. This quantity, computed for each node, is then averaged over all neuron types to yield a single global value, CC_{HC}.

Characteristic path length is defined as the mean of the shortest directed (i.e. axon to dendrite) path from a node to every other neuron type in the network. For example, Granule cells and CA1 Pyramidal cells are not in direct contact, so communication requires at least one intermediary; in fact, there are five two-step pathways (via types [19], [20], [44], [46], or [47]). Determining analogous distances from Granule cells to the other types in the network and averaging gives $CPL_{Granule}$=2.11, meaning that they can send information anywhere in the network in an average of just over two steps. Then, averaging this quantity over all 122 types yields a single global value, CPL_{HC}. Mathematically,

$$CPL_{HC} = \frac{1}{n} * \sum_{i=1}^{n} \left(\frac{1}{n} * \sum_{j=1}^{n} shortest\ path\ i,j \right)$$

where n is the number of nodes in the network, i is the set of presynaptic types, and j is the set of postsynaptic types. Neuron types that have axons and dendrites co-located within at least one parcel are self-connected and have a shortest path length to themselves of zero (e.g. the shortest path from CA1 Pyramidal cells to CA1 Pyramidal cells is 0); non-self-connected types require multi-step paths to communicate with themselves (e.g. traveling from Granule cells to Granule cells requires two steps).

Node degree is the number of connections made by a node (out-degree; OD), to a node (in-degree; ID), or the sum of these quantities (total-degree, also called degree centrality; TD). Again, Granule cells have 33 immediate neighbors ($OD_{Granule}$=33), and they are immediate neighbors to 26 other types ($ID_{Granule}$=26); $TD_{Granule}$=33+26=59. Self-connected neuron types thus contribute two connections to

189 their total-degree. A related measure, polarity, is defined as (ID–OD)/TD (Shih et al., 2015).

190

191 *Topology comparison analysis*

192 For six well-known network types, we generated 1,000 random networks identical in size to the HC
193 and compared their CC and CPL. The two metrics were then combined to measure the overall (i.e.
194 global and local) "communication cost." Specifically, the cost was computed as follows:

$$\text{Communication cost} = -\log_{10}(CC) + \log_{10}(CPL)$$

195 For each network type, the resulting cost was linearly scaled so that the reference network (HC) was
196 given unitary value.

197 The algorithms to produce the Erdős-Rényi (ER), lattice, ring, Watts-Strogatz (WS), Barabási-Albert
198 (BA), and Klemm-Eguílez (KE) networks were also implemented in MATLAB (open-source code:
199 github.com/Hippocampome-Org/GraphTheory) using published pseudo-code (Prettejohn et al., 2011).
200 Briefly, an ER network (Erdős and Rényi, 1960) is constrained only by its number of nodes and its
201 connection density; we used HC network values of 122 and 21.7%. These graphs were constructed by
202 considering all possible connections among the nodes and inserting them with probability equal to the
203 connection density. A square lattice network, in contrast, is heavily constrained by the number of
204 nodes, edges, and the fact that each node must be connected to its K nearest neighbors (where K is
205 the ratio between HC edges and nodes: 3,236/122=26.5). A ring network, a one-dimensional string of
206 nodes "bent" into circular form by joining the ends, is similarly constrained. Starting from a highly
207 clustered ring graph, WS (Watts and Strogatz, 1998) networks were created by considering each
208 connection for random rewiring with constant probability ($p_{rewiring}$=0.4) in order to introduce long-
209 distance (i.e. cross-network) edges. For BA scale-free networks (Barabási and Albert, 1999), we
210 started from an initial size of ten fully connected nodes and serially attached the remaining 112 nodes
211 to pre-existing nodes chosen with probability proportional to their OD in the growing network. This
212 preferential addition of new nodes to higher-degree nodes yields the desired power law distribution for

213 the final network degree, with the vast majority of nodes having very small OD and a select few types
214 having large OD. Finally, KE networks (Klemm and Eguiluz, 2002) are generated to obtain high CC
215 and low CPL (like WS networks), along with a scale-free OD distribution (like BA networks). The
216 algorithm is similar to that used for BA networks, but attachment of new nodes is preferentially biased
217 toward high-degree, highly clustered "active" nodes (Prettejohn et al., 2011).

218

219 *Modularity*

220 The HC modular, or community, structure was bared by computationally assigning neuron types into
221 non-overlapping groups to maximize within-community connectivity and minimize extra-modular
222 cabling. Community assignments are evaluated by a modularity score, Q, which quantifies the fraction
223 of connections in a module relative to those expected by chance (Newman, 2004). Practically, we use
224 BCT code based on a spectral algorithm that optimizes Q over possible HC divisions (Leicht and
225 Newman, 2008). The algorithm was run 100 times and the detected communities did not change.

226

227 *Rich club analysis*

228 Rich club (RC) analysis utilized a modified version of BCT code to identify cores of nodes that are
229 more highly connected to each other than expected by chance (Zhou and Mondragón, 2004; Colizza
230 et al., 2006; McAuley et al., 2007; van den Heuvel and Sporns, 2011). First, a connectivity fraction (C_f)
231 is computed for each degree level k from 1 to the maximum TD in the network (i.e. 114, for CA3c
232 Pyramidal cells) as the proportion of edges that connect nodes of degree>k relative to the maximum
233 number of edges that such nodes might share (Colizza et al., 2006). These C_f values are then
234 normalized relative to the average for a given k in a population of 1,000 random networks synthetically
235 generated to have fixed OD and ID distributions matching the HC. Raw p values were calculated at
236 each k based on the C_f percentile rank of HC within the population of 1,000 random networks.
237 Normalized C_f values that were significantly greater than 1 over a range of k's with p values smaller

than 0.05 after "false discovery rate" (FDR) multiple testing correction (Storey, 2002) were designated as members of RC tier I. The cutoff for inclusion in RC tier II was selected based on the relatively large C_f increase in HC between k=77 (C_f=0.630) and k=78 (C_f=0.766).

Absorption and driftness analyses

Shortest path lengths between neuron types were again measured using BCT. The number of paths of length *y* between all pairs of types may be found simultaneously by multiplying the unweighted connectivity matrix, M, by itself *y* times (e.g. the matrix entries obtained by calculating M^3 are the number of paths of exactly three steps between types). Absorption and driftness (Costa et al., 2011) values were also computed in MATLAB. The absorption metric simulates average random walks as a surrogate for dynamic activity in the network. In a given random walk from a starting neuron type to a destination, the walk progresses with equal probability to any of the connected types and continues until the target is reached. Averaging a large number of independent random walks mimics parallel propagation of activity over all possible paths connecting two neuron types. Driftness is calculated as the absorption value divided by the CPL for each pair of neuron types (Costa et al., 2011).

Connectivity superpattern and pattern profiles

At a local level, we investigated the configurations of connectivity (or lack thereof) for all groupings of three neuron types. In a circuit with 122 elements chosen three at a time without regard to order, this equates to a total of 295,240 combinatorial relationships. In one analysis, we examined connectivity "superpatterns" without distinguishing excitatory and inhibitory connections (i.e. the network was considered directed but unweighted); in a second, we studied the directed and weighted network "patterns." For the sake of interpretability, self-connections among types were not considered as differentiators in this analysis. Superpattern and pattern libraries and detection algorithms were built from scratch using MATLAB (github.com/Hippocampome-Org/GraphTheory).

Excitability scores (ES) quantify the net counterbalance of excitation versus inhibition occurring within a triad of neuron types. These scores are computed at each node in the pattern, then summed over the three nodes. If a node does not receive a connection from either of the two other nodes, its score is equal to its sign (+1 if excitatory node, -1 if inhibitory): this node is not amplified or dampened by the rest of the pattern. If a node receives a connection from one or both other node(s) in the pattern, its score equals its sign multiplied by 1.1 for each incoming excitatory connection, and by 0.9 for each incoming inhibitory connection. Explicit examples of this computation are included in the Results.

Patterns may or may not have a unique ES. Thus, for each ES, we also quantified the relative prevalence within the detected modules, so as to determine whether the underlying communities tended to utilize repeatedly certain sets of excitatory/inhibitory configurations. The relative importance of these interactions to a module is computed based on the number of times an ES appears within that module relative to the overall network.

Detection of motifs and anti-motifs

Analogously to the rich club analysis, counts of HC superpatterns and patterns were compared to a population of 1,000 random networks to find those that were significantly over- or under-utilized relative to expectancy, respectively called motifs and anti-motifs (Milo et al., 2002; Milo et al., 2004). These random networks were generated in parallel by selective edge swaps chosen stringently and conservatively so as to maintain the underlying spectrum of two-node (i.e. dimer) superpatterns and patterns. Specifically, the random networks preserved the HC number of excitatory (E) and inhibitory (I) nodes and connections; the number of E to E, E to I, I to E, and I to I connections; and the OD and ID of each node. Accordingly, each edge in the graph had a limited number of valid swap partners from which a suitable mate was randomly chosen. Fifty swapping passes were made over all edges in order to sufficiently scramble the original network.

The statistics employed for the motif/anti-motif analysis were similar to the RC analysis: raw p values

for each pattern were based on the percentile rank of the HC count within the random population. Patterns with percentile ranks >95 (meaning that the pattern appeared in the HC more than in 95% of the 1,000 random networks) underwent multiple testing corrections to determine whether they constituted statistically significant motifs. Similarly, patterns with percentile ranks <5 underwent testing to identify anti-motifs. Adjusted p-values were calculated with the step-down "min P" procedure (Westfall and Young, 1993), and patterns with corrected values < 0.05 were deemed significant.

Pairwise correlation analysis

Pairwise correlation were evaluated among 315 properties across the 88 neuron types in the DG, CA3, CA2, and CA1 sub-regions. In addition to connectivity properties detailed herein (degree, strength, polarity, and usage of superpatterns/patterns), we examined morphological features (e.g. somatic, axonal, and dendritic locations, as well as the projecting or local nature of axons), molecular markers (e.g. expression, or lack thereof, of various calcium-binding proteins, neuropeptides, or receptors), and assorted passive and spiking electrophysiological parameters (e.g. input resistance, fast or slow membrane time constants, action potential width). Neuron types from subiculum and EC were excluded from this analysis due to the scarcity of available molecular and electrophysiological information. Direct and inverse relationships between properties were detected using 2x2 contingency matrices, and p-values were calculated with Barnard's exact test (Lydersen et al., 2009).

Results

In building the neuron type connectome of the hippocampal formation, we extracted information for 167 known connections and 68 non-connections from the literature. For the remaining 14,649 type pairs (i.e. 122^2-235 known connections or non-connections), we calculated the spatially-based potential connectivity, which excluded the possibility of connections for 11,580 pairs of neuron types. Consequently, 3,069 potential connections were combined with 167 known connections to obtain the

HC network explored here: a graph of 38 excitatory and 84 inhibitory neuron types (nodes) interlinked by 3,236 edges (1,216 excitatory and 2,020 inhibitory; full connectivity data may be downloaded from Hippocampome.org/netlist).

A highly specialized topology

We first compared the HC clustering coefficient and characteristic path length to those of six identically-sized, well-known network types (ER, BA, WS, KE, rings, and lattices). Because of the relatively small size of the graphs, CC and CPL showed little variance over the 1,000 randomly generated variants of each network type (Fig. 2A). CC is indicative of the tendency of nodes to gather in tightly knit groups that may correspond to functional processing units, while CPL reveals the relative expanse of the network. Together, these metrics characterize network topology in terms of communication cost: large-world networks (Boccaletti et al., 2006) contain densely connected groupings of nearby nodes, but remote nodes are only reachable by paths with many steps (dark green background shading in Fig. 2A). At the opposite extreme, uniform random networks have low CC and CPL because of the arbitrary placement of their edges (dark gray shading). Scale-free networks (gold shading) and small-world networks (blue shading) represent two popular mixed cases, with low CC/high CPL and high CC/low CPL respectively. HC displays both high CC, analogous to rings and lattices, and low CPL comparable to ER random networks. This suggests that hippocampal neuron types rapidly combine information across short path lengths into targeted areas, where specialized processing occur within tightly interconnected circuits. In fact, not only is HC classifiable as a small-world network, but its combined global and local communication cost is lower than any of the other tested networks (Fig. 2B). Moreover, when PC connections were weighted ten times more heavily than other edges, both CPL and the overall communication cost further decreased by 25%.

Significant community structure

The organization of HC connectivity can be visually inspected on a circular graph (Fig. 3A). The innate community structure is identified by grouping the 122 neuron types in order to maximize intra-modular wiring and minimize inter-modular wiring. The modularity score Q measures the effectiveness of the resulting grouping, with values of $Q \approx 0$ indicating randomness (i.e. the groupings are equally good, or poor) and, in practice, $Q > 0.3$ pointing to noteworthy community structure (Newman, 2004). The HC network is optimally subdivided into four modules with $Q = 0.53$. Connections between neuron types within one of these communities account for 81% (2,622/3,236) of all graph edges, and the average connection density of the four modules is 0.675, dwarfing the between-module connection density of 0.041 (614/3,236). Interestingly, the communities do not themselves partition into smaller submodules as the average Q score for each of the modules is 0.09 (Fig. 3B). Thus, the four detected communities are the major, high-level processing units of the network.

Even though axons of neuron types frequently cross sub-region boundaries to form connections (i.e. 33/122 types project to different sub-regions from their soma location), the detected communities closely aligned with DG, CA3, CA1, and EC (the first three are shown in Fig. 3C), the most-highly-studied sub-regions of the hippocampal formation. These sub-regions are also the major players in the trisynaptic loop (TSL) relay (highlighted as thick, brightly colored chords in Fig. 3A). The “DG module” identified by this analysis contained all 18 DG types, along with one of the CA1 types that projects to DG (i.e. CA1 Neurogliaform Projecting). The “CA3 module” included all 25 types from CA3 and four out of five types from less-researched CA2. The exception, CA2 Bistratified cells, belonged to the “CA1 module,” along with the remaining 39 CA1 types and SUB CA1-Projecting Pyramidal cells. Finally, the “EC module” contained all 31 EC types and the other two subicular neuron types. Notably, this core modular structure was revealed even without differentially weighting the PC connections.

Degree distribution and hubs

362 The numbers of connections made and received by a neuron type respectively correspond to out- and
363 in-degrees (Fig. 4A), and types with a relatively high total-degree may be generally considered
364 network hubs (van den Heuvel and Sporns, 2013). The HC OD distribution (thin red columns) has
365 both a more asymmetric and a more heavily tailed spread than the ID distribution (thick blue columns),
366 as quantified respectively by skewness and kurtosis values. While both distributions have positive
367 skewness, indicating a right-shifted distribution attributable to the presence of network hubs, the
368 skewness of the OD distribution is more than four times larger. More strikingly, the OD kurtosis (2.87)
369 denotes a much heavier tail than is found with the in-degree distribution, whose negative value close
370 to zero indicates near-normal, if not thinner-than-normal, tails (Pearson, 1905; Westfall, 2014).

371 Altogether, this evidence points to an axonal architecture that is both anomalous and nonrandom in
372 contrast to a relatively ordinary dendritic architecture. The peculiarity in the axonal distribution is
373 accentuated by breaking down the data by neuron types that project to another sub-region
374 (Hippocampome.org/morphology) versus those with only local axons (Fig. 4B). The projecting types
375 (thick green columns; n=33) show a heavy, right tail versus the light, left tail of the local types (thin
376 gray columns; n=89). These tails indicate, separately, the presence of neuron types that serve as
377 highly connected hubs and types that are decidedly particular in the connections they form.

378 The top and bottom neuron types by TD may be respectively considered global hubs and anti-hubs
379 (Table 2). The list signals the importance of the CA3 module and highlights its central role in the TSL
380 circuit: pyramidal cells from CA3, CA3c, and CA2 are three of the four most connected neuron types in
381 the network. The other, CA1 Back-Projection cells, is an interneuron type in CA1 with axons that
382 project upstream to CA3 (and DG), opposite to the TSL flow. Notably, Granule cells are not a global
383 hub based on pure topology (i.e. they are only the 43rd most connected neuron type), but they become
384 the third most critical type in the 10x PC weighted network. Thus Granule cells do not influence a large
385 number of neuron types; rather, their importance in the HC is largely due to their relative abundance.

386 Certain neuron types are global hubs due to a high OD even with a low ID (i.e. they have a dominant
387 axonal architecture); others are more balanced. The top four global hubs have OD>>ID (i.e. a large,

388 negative polarity) and constitute network divergence points. Global anti-hubs, with positive polarities,
389 like axo-axonic cells, basket cells, and interneuron specific cells, indicate selected targets of
390 information convergence. In contrast, provincial hubs, which by definition do not project outside of
391 their module, are highly connected within the module and serve as critical traffic directors (van den
392 Heuvel and Sporns, 2013). The top provincial hubs in the DG, CA3, and CA1 modules (bottom portion
393 of Table 2) are again not restricted to a certain polarity. In DG, MOLAX cells tend to funnel information
394 to specific points within the DG, but CA1 Oriens-Bistratified cells distribute information widely to 36 out
395 of 41 CA1-module types; CA3 Bistratified and Ivy cells have relatively balanced, neutral polarities.

396

397 **Rich and ultra-rich clubs**

398 Rich club analysis showed that the global hubs are significantly more connected amongst each other
399 than could be expected by chance. In fact, all nodes with TD≥55 (not just the top global hubs), have
400 statistically higher interconnectivity than in equivalent random networks (Fig. 5A; normalized data>1).
401 Although nearly half (56/122; 45.9%) of the neuron types belong to this RC I (both light- and dark-
402 purple shaded regions of Fig. 5A), the top 8 hubs from Table 2 are also members of a tighter “richest
403 of the rich” club within (RC II; dark-purple shading only), boasting the highest edge density of 76%
404 (Fig. 5B). Members of RC I consisted of types from all four modules (Fig. 5C), but a disproportionate
405 number (42/56) came from CA1 and EC, as these modules are densely connected and have the most
406 nodes. Interestingly, all RC II types were located in CA3 and CA1 (Fig. 5D).

407

408 **Robustness to random failures**

409 Any two neuron types within a network can typically connect through multiple alternative pathways,
410 providing redundancy for information flow. The maximum shortest pathway length in HC, five steps,

was only found between certain DG and EC types, a route that requires upstream travel against TSL current (Fig. 6A). Approximately two-thirds of all pairs of neuron types are connected by two steps or fewer, and nearly 95% by three (Fig. 6B, percentage labels). Moreover, increasing the length of possible paths by just a single step raises the number of available alternates by successive orders of magnitude (Fig. 6B, blue columns). For example, there are on average 5.81 available two-step pathways in HC between two neuron types. While certain pairs have no such pathways (e.g. from DG to EC), others have many possible two-step routes at their disposal (Fig. 6C).

The absorption value for a pair of neuron types is the average length of *all* paths (the length of a "random walk") between them (Fig. 6D). The overall average absorption of HC is 230.5. While the out-absorption vectors (i.e. the rows in the matrix) are relatively similar across all nodes, the in-absorption vectors (columns) are highly specific to a given node. Therefore, neuron types are activated with just as much ease or difficulty from any part of the network, depending primarily on the dendritic architecture of the type and its close neighbors. CA2 and subiculum, being hard to reach with few connections arriving at a select few types, and EC, due to overall unidirectional information flow through the TSL, have high in-absorptions. Driftness corresponds to the absorption normalized by the shortest path lengths between the types (Fig. 6E). Intra-CA2 and intra-EC values are again high, but those for most other type pairs are low, indicating the existence of multiple pathways of similar scale to the shortest path. This feature suggests that the HC network could continue to operate at near-optimal levels after insult to random neuron types and connections. Notably, however, while the absorption values are unchanged when accounting for 10x PC weighting, the overall average driftness increases from 111.8 to 170.0. Thus, the "shortest" path between many types (i.e. through the PCs) is both unique and irreplaceable, and the PCs represent points of vulnerability.

Characteristic connectivity superpattern profile

To examine the local interactions of neuron types, we consider all 16 possible ways in which three

436 unweighted nodes can interrelate: 13 where all three nodes directly participate in at least one
437 connection (Fig. 7A, graphs labeled A through M) and 3 cases with at least one node disconnected
438 from the others (labeled -A, -B, and -C). The frequency of occurrence for these 16 building blocks
439 constitutes the HC *connectivity superpattern profile* (Fig. 7B). An absolute majority of the 295,240
440 trimer occurrences in HC (248,118 or 84%) involve at least one disconnected type. Of the fully
441 connected trimers, the superpattern consisting of a single uplinked mutual dyad (superpattern F; name
442 modified from Milo et al., 2002) and the single input module (superpattern C; named after Zaslaver et
443 al., 2002; Alon, 2007) represent nearly a collective one third (15,443/47,122; 32.8%). Most interactions
444 take place intermodularly (Fig. 7C) involving projecting neuron types. In both F and C, a single node
445 disperses information to two neuron types that do not interact with each other, with superpattern F
446 receiving direct feedback from one partner and C containing no feedback from either partner. In
447 contrast, superpattern I, a similar structure containing a chain of two mutual dyads, wherein both
448 receivers of the dispersed signal provide direct feedback, is one of the least frequent. These
449 observations point to a strong, net-unidirectional information flow between modules, often in the TSL
450 direction. Furthermore, as the internal connection densities of trimer superpatterns increase (i.e.
451 across vertical, black dotted lines in Fig. 7C), with the exception of F and C, intramodular utilization
452 also increases, underscoring the importance of signal fine-tuning for local microcircuit interactions.

453 Next we analyzed the breakdown of superpatterns in the CA1 module as utilized by Pyramidal cells
454 versus interneurons (Fig. 7D, blue line). Though many CA1 interneurons interact primarily with
455 pyramidal neurons, many others, including calretinin-positive (CR+) (Gulyás et al., 1996) and
456 vasoactive intestinal peptide-positive (VIP+) (Acsády et al., 1996) cells do not, and the interactions of
457 many other interneuron types are unknown. Pyramidal cells dominate the usage of all superpatterns
458 except C, E (a feedforward loop), and K (a double uplinked mutual dyad). Interestingly, in CA1, such
459 diminution is specifically attributable to an elevated employment of these trimers by perisomatic-
460 targeting (PST) interneurons, namely CA1 Axo-axonic cells, Horizontal Axo-axonic cells, Basket cells,
461 Basket CCK+ cells, and Horizontal Basket cells (Fig. 7D, red dotted line).

462

Weighted pattern profile and neuron type fingerprint analysis

The number of distinct connectivity trimers grows substantially when distinguishing excitatory and inhibitory nodes. After considering rotational symmetry, 104 possible interaction patterns exist between three nodes: 86 fully connected and 18 with at least one disconnected node. For example, eight connectivity patterns correspond to superpattern F, the single uplinked mutual dyad (Fig. 8A). The excitability score ES captures the overall excitatory or inhibitory nature of a pattern by accounting for the net amplification and dampening of each node by their connected partners. Consider, for instance, pattern F4: a mutually interacting pair of excitatory and inhibitory types, with the former being "uplinked" to a second inhibitory type. Every node in F4 receives a connection from another node and is scored independently. The score of the inhibitory node on the right of the pattern (when rotated as in Fig. 8A) is equal to -1.1 because the original value, -1, is amplified (i.e. multiplied) by an inbound excitatory signal. The score of the node at the bottom of the pattern, another inhibitory type that receives excitation, is identical. At the top of the pattern, the original value of this excitatory type (+1) is dampened by an inbound inhibitory edge from the bottom node, yielding a value of 0.9. Summing the scores from all three types gives an overall ES = (-1.1) + (-1.1) + (0.9) = -1.3 for this pattern.

The ES distribution for all 104 trimer patterns has four narrow peaks determined by the number of excitatory or inhibitory nodes therein; accordingly, trimer neuron type patterns may be categorized as strongly inhibitory, mildly inhibitory (e.g. pattern F4, which has two inhibitory types), mildly excitatory, and strongly excitatory. The abundance of inhibitory types over excitatory types in the DG, CA3, and CA1 modules yields higher usages of strongly and mildly inhibitory patterns, consistent with the known diversity of GABAergic interneurons (Fig. 8B). Two patterns, L8 and F4, are particularly prominent in certain modules. L8, the all-inhibitory version of superpattern L (refer back to Fig. 7A) consisting of a feedback loop between two mutual dyads, is used ubiquitously in CA1 to fine-tune inhibition. In contrast, the pervasiveness of F4 in CA3 (and, in fact, the whole HC) is almost entirely due to CA3 Pyramidal cells (Fig. 8C), which heavily employ this pattern to disperse information simultaneously to both CA3 interneurons (many of which supply direct feedback) and CA1 interneurons via the Schaffer collaterals (no direct feedback). In fact, pattern 'fingerprint' profiling reveals that F4 is by far the

dominant class of interactions for CA3 Pyramidal cells (Fig. 8D, brown data series; note log radial scale). The overall HC usage of all 86 connected patterns (blue shading) is shown for comparison.

Moreover, HC conspicuously underutilizes superpattern G, along with each of the patterns G1-G4 (45 total interactions out of 295,240). Indeed, these patterns, corresponding to a unidirectional feedback loop with no reciprocal connections, are avoided in favor of other structural blocks. When two unidirectional connections transmit signals forward along a chain in HC, nodes 1 and 3 are rarely connected by unidirectional feedback as in G (0.5% of such cases); instead, they are either unconnected in a three-node chain (superpattern B; 38.5%), connected by a feedforward link (superpattern E; 49.8%), or connected by a reciprocal edge that serves both feedback and feedforward purposes (superpattern J; 11.2%). This strikingly uneven distribution is consistent with forward-directional circuitry where feedback tends to be relatively immediate and curbed (e.g. in the form of a reciprocal edge) or else drawn out over a more global scale. Comparing the counts and circuit locations of feedforward and feedback loops (superpatterns E and G, respectively), along with specific examples and tabulated interpretations, clearly illustrates this trend (Fig. 9). Note that, while only four feedback patterns exist due to rotational symmetry, there are 8 feedforward patterns.

Motifs and anti-motifs

To identify significantly over- or under-represented subcircuits, we benchmarked the HC networks to random graphs in which global topology was obliterated, but the underlying composition of all dimers was preserved. Surprisingly, superpattern topology was the most important factor in determining whether a pattern was a motif or an anti-motif (Fig. 10A). In other words, most superpatterns (13/16) are either motifs or anti-motifs, independent of the excitatory/inhibitory make-up of their nodes. Only the three-node chain, the single downlink to a mutual dyad, and the single uplinked mutual dyad (superpatterns B, D, and F) contained a mixture of motifs and anti-motifs (stacked green and red columns). For the others, the connectivity itself was either over- or under-employed relative to the expectation based on HC dimer distribution. Patterns belonging to D (single downlink to a mutual

516 dyad), G (feedback loop), and I (chain of two mutual dyads) were severely underutilized, but patterns -
517 B (disconnected single edge), -A (disconnected mutual dyad), E (feedforward loop), H (double
518 downlink to a mutual dyad), K (double uplinked mutual dyad), L (feedback with two mutual dyads), and
519 M (fully connected triad) were all strong motifs. These results were robust to PC weighting.
520 Additionally, motifs and anti-motifs were module-specific (Fig. 10B-D). The DG module contained a
521 mixture of motif and anti-motifs for many superpatterns. Less-densely connected superpatterns,
522 including simple regulation (name from Alon, 2007), three-node chain, single input module, and single
523 downlink to a mutual dyad (superpatterns A through D) were underutilized in CA3; instead, these
524 superpatterns tended to be slightly over-utilized in CA1, where F and G were anti-motifs.

525

526 **Pairwise correlations**

527 For the 88 neuron types not located in EC or subiculum, we tested the interactions among 315
528 connectivity, morphological, molecular, and electrophysiological properties and detected 14,217
529 (14.3%) significant correlations ($p<0.05$). These results fell across a spectrum of novelty, and the more
530 interesting outcomes are presented here.

531 Like in the motif analysis, sub-regional differences in the usage of superpatterns and patterns were
532 revealed. DG types have high participation (i.e. relative to other sub-regions) in three-node chains
533 (superpattern B; $p<0.02$) but shun dense, highly connected superpatterns, including I (chain of two
534 mutual dyads; $p<0.002$), J (single point feedforward and feedback loops; $p<0.006$), K (double uplinked
535 mutual dyad; $p<0.00002$), L (feedback with two mutual dyads; $p<0.00006$), and M (fully connected
536 triad; $p<0.0005$). Interestingly, CA3 and CA1 do not share parallel high or low participation in any
537 superpattern or pattern. Instead, one pattern is highly used in CA1 but avoided in CA3 and one pattern
538 displays the opposite trend. Pattern H6, where an interneuron acts as a single input module dispersing
539 information to two interneuron recipients with reciprocal feedback between them, is highly utilized in
540 CA1 and under-employed in CA3. Contrarily, pattern L3, a reciprocal edge between two excitatory
541 types, one of which is connected reciprocally with an interneuron and the other of which receives uni-

542 directional information from that interneuron, is avoided in CA1 but highly used in CA3. This
543 connectivity pattern is especially utilized by CA3 and CA3c Pyramidal cells to communicate with each
544 other and with a third (interneuron) partner.

545 Pairwise contingency analysis also detected a set of characteristics differentiating projecting from local
546 neurons. Projecting types participate highly in superpatterns where information converges to a single
547 point onward through the TSL ($p<0.0003$): superpattern A (simple regulation) and superpattern E
548 (feedforward loops). Conversely, projecting types use sparingly superpattern C (single input module)
549 and particularly pattern C5 ($p<0.0003$), which is disperse excitation to two inhibitory nodes. CA1 Back-
550 Projection cells, a major GABAergic projecting type, are the exception. This neuron type primarily
551 interacts with other hippocampal interneurons and makes use of patterns C6 (inhibitory dispersal to
552 two other GABAergic types) and F8 (Fig. 8A) more than any other neuron type.

553 Lastly, connectivity was clearly correlated with molecular expression (Hippocampome.org/markers).
554 While the correlation between subcircuits involving only inhibitory types (e.g. from superpatterns A, D,
555 I, and L) with expression of VIP+ and CR+ (two markers of interneuron-specific interneurons) was
556 expected, other observations were not. For example, even though somatostatin is not associated with
557 interneuron-specific interneurons, somatostatin-positive (SOM+) cell types also tend to interact in
558 groupings with two other GABAergic types (sometimes, but not always, with interneuron-specific
559 types). More specifically, SOM+ types are among the top users of the all-inhibitory versions of
560 superpatterns D, E, F, H, J, L, and M. In addition, neurons expressing parvalbumin (including
561 perisomatic-targeting basket and axo-axonic cells) participate copiously in superpattern C (single input
562 module), but sparingly in superpatterns B (three-node chain), D (single downlink to a mutual dyad), J
563 (a single point feedforward and feedback loop), and M (fully connected triad).

564

565 **Sensitivity to future additions or subtractions of neuron types**

566 Finally, to examine the robustness of our results to reasonable changes in network size and
567 composition, we reran all analyses on two modified networks. First, we eliminated 26 of the 122
568 neuron types (asterisks in Table 1), along with their connections, that were either not well known (e.g.
569 described by a single peer-reviewed publication) or contained no or sparse molecular marker and
570 electrophysiological evidence. In the second network, we added 23 new neuron types that are
571 currently being annotated for inclusion in future versions of Hippocampome.org. Remarkably, analysis
572 of both networks yielded results very similar to those reported here for the network of 122 types.
573 Specifically, connection density, CPL, CC, and scaled communication cost were all within 4% of their
574 HC values. More complex analyses (e.g. rich club and motifs) were similarly dependable.

575

576 **Discussion**

577 Knowledge about synaptic connectivity between identified neuron types in the hippocampal formation
578 is currently quite scant: empirical information on the presence or absence of synapses is available for
579 less than 1.6% of all possible neuron type pairs. These limited data, however, can be supplemented
580 by leveraging spatially co-aligned axonal and dendritic patterns based on the evidence annotated in
581 Hippocampome.org. Although axonal-dendritic co-location does not guarantee synaptic presence,
582 applying the original, neuron-type version of Peters' rule at least reveals the potential connectivity of
583 the full hippocampal circuitry. While the concept of potential connectivity is extensible in other parts of
584 the brain, it is particularly pertinent in the hippocampus due to its superior structural plasticity (Leuner
585 and Gould, 2010). In particular, in this region, the lack of synapses between neurons at any given
586 moment may not necessarily foreshadow the absence of connection at a different time.

587 This level of description of the rodent cerebro-hippocampal cortex complements (and fills a gap
588 between) previous large-scale syntheses of tract-tracing studies (Burns and Young, 2000; van Strien
589 et al., 2009) and sparse synaptic sampling (Druckmann et al., 2014). In fact, this effort represents the
590 first comprehensive, literature-based neuron-type circuitry inventory for a mammalian cortical region.

591 Thus, we began to unravel the structural complexity of the hippocampal network through graph theory
592 analyses, shedding light on the functional roles of the component neuron types.

593 Although networks are quantitatively differentiable according to myriad metrics, two of the most
594 topologically illustrative are CC and CPL (Watts and Strogatz, 1998). We first identified and quantified
595 the specialized topology that brings about higher efficiency and lower overall communication cost in
596 HC than in any equivalent, well-studied network type. Small-world networks, in particular, have been
597 researched and applied fashionably to brain networks for decades (Hilgetag and Goulas, 2016), but
598 we detected significantly higher CC than in equivalent WS networks. The in-built capacity for rapid
599 response times and precise processing, common elsewhere in the brain (Latora and Marchiori, 2001;
600 Bassett and Bullmore, 2006; Rubinov and Sporns, 2010; Mišić et al., 2014), might be especially
601 relevant to the demands of the hippocampus, where the tasks of memory consolidation, retrieval,
602 cognitive navigation, and path-finding have inherent temporal and spatial constraints.

603 Next, we exposed a significant modular substructure comprising four densely intra-connected
604 communities. It is worth noting that CA2 and the subiculum, the two hippocampal formation sub-
605 regions with the fewest known neuron types (five and three, respectively), are currently subsumed into
606 communities dominated by other sub-regions. CA2 types are split into the CA3 and CA1 modules;
607 subicular types are divided among CA1 and EC. As future knowledge in these areas increases,
608 presumably hailing a proliferation in interneuron diversity, one or both of these sub-regions might
609 become independent modules.

610 Regardless, the major high-traffic links between the sub-regionally-based communities recapitulate
611 the TSL and various shortcuts through it. This excitatory relay includes the perforant pathway (PP; grid
612 and border cells from EC layer II to DG and CA3), the temporoammonic pathway (head direction and
613 border cells from EC layer III to CA1), mossy fibers (from DG Granule cells to CA3), Schaffer
614 collaterals (from CA3 Pyramidal cells to CA1), and the nameless projection from CA1 to EC layer V
615 (Amaral and Lavenex, 2007; van Strien et al., 2009). Although the functional ramifications of these

individual conduits are not yet fully understood, in a loop-heavy network that lacks discrete beginning and endpoints, the detected modules likely act as processing stations regulated by dense intra-modular connections (both excitatory and inhibitory). For example, though most studies of the PP focus on the well-known glutamatergic-to-glutamatergic connections onto Granule cell dendrites, feedforward inhibition also plays a major role in controlling information processing in DG (Ferrante et al., 2009). As we have shown, the PP can also affect DG interneurons such as MOPP and Neurogliaform cells (pattern E2 in Fig. 9). Under physiological conditions, these parallel routes might selectively respond to particular oscillatory input frequencies from EC reflecting different behavioral states (Tateno et al., 2007; Akam and Kullmann, 2010; Ewell and Jones, 2010; Jones and McHugh, 2011). Novelty, for example, induces a slight decrease in Granule cell firing rates concomitant with increased DG interneuron activity (Nitz and McNaughton, 2004).

Analysis of out-degree and in-degree distributions revealed that the peculiar HC topology was largely due to its axonal architecture while the dendritic circuitry was fairly unremarkable. This result is consistent with the recent finding that the computational load of neurons is unrelated to their in-degree (Timme et al., 2016); instead, neurons that process large amounts of information tend to receive connections from high OD neurons. The axonal distribution further pointed to anti-hub and hub neuron types that utilized highly specific or largely blind targeting, respectively. Hubs are notable because, by directly connecting to many neuron types that are themselves neighbors, they violate typical tenets of wiring minimization (Chklovskii et al., 2002; Chklovskii and Koulakov, 2004; Chen et al., 2006; Bullmore and Sporns, 2012). In fact, both the construction of these superfluous, often long-distance connections and the regular handling of a disproportionately large volume of traffic come at a high cost of energy. At the same time, these nodes facilitate the integration of distributed neural activity and are well situated to integrate the network modules. Such double-edged nature justifies the “high cost, high value” characterization of these circuit elements (van den Heuvel and Sporns, 2013).

While quantification of modularity yielded informative but non-overlapping groupings of HC neuron types, the rich club analysis produced a hierarchical ordering of importance of each type to the

network. Rich clubs also have been detected in other parts of the brain across several species (van den Heuvel and Sporns, 2011; Harriger et al., 2012; Shanahan et al., 2013; Binicewicz et al., 2015). We identified two nested rich clubs that are likely to route much of the network traffic (Mišić et al., 2014) within the hippocampal formation. Like hubs, this feature accentuates a departure from the parsimonious wiring typically observed in neural systems, but the paths between these critical types provide a highly efficient network core with built-in protection against neurodegeneration. Members of these rich clubs, including the global hubs, are potentially vulnerable to targeted attacks: damaging all neurons within one of these types could lower network efficiency and increase processing times, possibly impairing storage and retrieval functionality. Interestingly, these same types tend to be particularly abundant in terms of cell numerosity, with principal cells present in quantities up to 10 times higher than other neuron types (Bezaire and Soltesz, 2013), thus providing a certain level of resistance against random neurodegeneration. More generally, we showed that the plethora of alternate pathways available in the circuit serves as a second countermeasure.

Finally, we analyzed the superpattern and pattern building blocks responsible for the local interactions that enable global functionality. Three-node subgraphs have attracted considerable attention for their role in complex networks across disciplines (Milo et al., 2002; Shen-Orr et al., 2002; Milo et al., 2004), including neuroscience (Sporns and Kötter, 2004; Song et al., 2005; Santana et al., 2011; Binicewicz et al., 2015). They have been specifically studied in the hippocampus with focus directed at DG Mossy cells and unidentified hilar interneurons (Larimer and Strowbridge, 2008) and among recurrent connections of CA3 pyramidal cells (Guzman et al., 2016). Building on this well-defined framework, we added excitatory/inhibitory weights and identified connectivity pattern relations among HC neuron types. In truth, the empirical characterization of even simple (e.g. two-node) interactions between excitatory and inhibitory cells is still vastly incomplete. Recent recordings from more than 500 pyramidal cells and 1,500 GABAergic neurons in the mouse neocortex delineated fifteen interneuron types that could be grouped based on broad connectivity preferences (Jiang et al., 2015). One group preferentially formed synapses with pyramidal neurons; another, referred to as “master regulators,” connected nonspecifically to all types in proximity of their axons; two additional groups contained

669 interneuron specific (IS) cells that synapsed primarily with other interneurons of the same or of
670 different types, respectively. When these interactions are extended to include a third party (i.e.
671 trimers), the functional implications are more complex. IS cells, in particular, have recently been the
672 subject of much study for their role in disinhibition. Specifically, IS cells can influence principal neurons
673 by inhibiting other GABAergic interneurons (Pi et al., 2013; Jiang et al, 2015). In the cortex, this type
674 of circuit control has been linked to enhanced plasticity (Fu et al., 2015) and shown to affect social
675 behavior (Yizhar et al., 2011), sensorimotor integration (Lee et al., 2013), attention (Vogels and
676 Abbott, 2009; Sridharan and Knudsen, 2014; Zhang et al., 2014), and associative learning and
677 memory (Letzkus et al., 2011; Letzkus et al., 2015). The specific involvement of the hippocampus in
678 many of the above functions makes these connectivity patterns particularly worthy of study.

679 On a related note, the excitability scores computed for each patterns only capture the overall
680 excitatory/inhibitory nature of a structurally defined trimer. In actuality, each trimer can produce
681 multiple functional states that are affected by the degree of activation, delays in signal propagation,
682 the surrounding neural context, and the behavioral state of the organism (Sporns and Kötter, 2004).
683 Those various functional states of patterns and superpatterns are not analyzed here.

684 Further meaningful interpretation of our results was hindered by two main factors, both imputable to
685 data incompleteness. First, the neuron types identified in HC are limited to the information available in
686 the literature. While certain hippocampal areas are well studied (e.g. CA1), other domains, including
687 CA2, subiculum, and entorhinal GABAergic neurons are still under-researched. Other parts of the
688 subicular complex, including the prosubiculum, presubiculum, postsubiculum, and parasubiculum, are
689 not tracked in version 1.0 of Hippocampome.org. Though morphologically based neuronal-type
690 information was recently reported for the presubiculum (Nassar et al., 2015), on the whole, the
691 breadth of knowledge within these additional areas is relatively narrow. As the scientific community
692 overcomes these shortcomings, the published evidence and Hippocampome.org will grow, which will
693 result in additions and alterations to the connectivity. This accumulating knowledge could impact some
694 of the HC circuit properties described herein. To assess and mitigate this issue, we repeated the

695 analyses on modified (reduced and expanded) networks, and concluded that the main network
696 properties of HC are innate to the well-known, constituent neuron types and unshaken by reasonable
697 additions or deletions.

698 The second hindrance is the lack of connection weights beyond the binary differentiation of
699 glutamatergic and GABAergic types. A comprehensive solution of this problem requires quantitatively
700 estimating both the counts for each neuron type and the corresponding axonal and dendritic length
701 distributions. Ideally, cell counts would be determined from absolute, stereology-derived numbers for
702 each morphologically defined neuron type, but relative ratios of molecularly-defined subpopulations
703 across anatomical parcels could already be useful. These challenging experimental tasks are
704 complicated further by variation across rodent species, strains, ages, sexes, and anatomical axes.
705 Nevertheless, it is generally assumed that principal cells dominate the relative abundances of other
706 neuron types by an order of magnitude (Bezaire and Soltesz, 2013), with experimental observations
707 ranging from 89% of the hippocampal neuron population as a whole (Woodson et al., 1989) to 93%
708 within CA1 (Aika et al., 1994). Accordingly, we also carried out the graph theory analyses with
709 principal cell connections weighted as +10. Remarkably, our conclusions were largely unchanged and,
710 in many cases detailed herein, their significance was even amplified. In addition to obtaining counts
711 for the neuron types, weighting for connections should also be based on measuring the three-
712 dimensional overlap of the neurite trees of each type. However, this approach is currently unfeasible
713 as three-dimensional reconstructions (e.g. from NeuroMorpho.Org) are only available for a small
714 fraction of neuron types. Lastly, the expression levels of the primary neurotransmitters, as well as the
715 prevalence of membrane receptor proteins in distinct post-synaptic cell types, also play a role in
716 weighting the connections. Though this information, too, is currently lacking, appropriate data can be
717 included in the future to extend potential connectivity analyses beyond binary values.

718 With the set of tools deployed in this work, future updates to the connectome (through addition,
719 merging, splitting, and weighting of nodes and edges, or through augmentation of known connectivity)
720 can be analyzed in relatively short order. Furthermore, as information accumulates about aging and

721 disease states, the analyses can be repeated with a comparative bent. Extending the foundational
722 results presented here with the expected continuous growth of data will progressively improve our
723 understanding of how network architecture mediates hippocampal function and dysfunction.

724

725 **References**

726 Acsády L, Görcs TJ, Freund TF (1996) Different populations of vasoactive intestinal polypeptide-
727 immunoreactive interneurons are specialized to control pyramidal cells or interneurons in the
728 hippocampus. Neuroscience 73:317-334.

729 Aika Y, Ren JQ, Kosaka K, Kosaka T (1994) Quantitative analysis of GABA-like-immunoreactive and
730 parvalbumin-containing neurons in the CA1 region of the rat hippocampus using a stereological
731 method, the disector. Exp Brain Res 99:267-276.

732 Akam T, Kullmann DM (2010) Oscillations and filtering networks support flexible routing of information.
733 Neuron 67:308-320.

734 Alon U (2007) Network motifs: theory and experimental approaches. Nat Rev Genet 8:450-461.

735 Amaral DG, Lavenex P (2007) Hippocampal neuroanatomy. In: The hippocampus book (Andersen P,
736 Morris R, Amaral D, Bliss T, O'Keefe J, ed), pp37-114. New York: Oxford UP.

737 Ascoli GA, Donohue DE, Halavi M (2007) NeuroMorpho.Org: a central resource for neuronal
738 morphologies. J Neurosci 27:9247-9251.

739 Bandeira F, Lent R, Herculano-Houzel S (2009) Changing numbers of neuronal and non-neuronal
740 cells underlie postnatal brain growth in the rat. Proc Natl Acad Sci USA 106:14108-14113.

741 Barabási AL, Albert R (1999) Emergence of scaling in random networks. Science 286:509-512.

742 Bassett DS, Bullmore ED (2006) Small-world brain networks. The Neuroscientist 12:512-523.

743 Bausch SB, He S, Petrova Y, Wang XM, McNamara JO (2006) Plasticity of both excitatory and
744 inhibitory synapses is associated with seizures induced by removal of chronic blockade of activity in
745 cultured hippocampus. J Neurophysiol 96:2151-2167.

746 Bezaire MJ, Soltesz I (2013) Quantitative assessment of CA1 local circuits: Knowledge base for
747 interneuron-pyramidal cell connectivity. Hippocampus 23:751-785.

748 Binicewicz FZ, van Strien NM, Wadman WJ, van den Heuvel MP, Cappaert NL (2015) Graph analysis
749 of the anatomical network organization of the hippocampal formation and parahippocampal region in
750 the rat. Brain Struct Func 25:1-5.

751 Boccaletti S, Latora V, Moreno Y, Chavez M, Hwang DU (2006) Complex networks: Structure and
752 dynamics. Phys Rep 424:175-308.

753 Braitenberg V, Schüz A (1991) Anatomy of the Cortex: Statistics and Geometry. Berlin: Springer-
754 Verlag.

755 Bullmore E, Sporns O (2009) Complex brain networks: graph theoretical analysis of structural and
756 functional systems. Nat Rev Neurosci 10:186-198.

757 Bullmore E, Sporns O (2012) The economy of brain network organization. Nat Rev Neurosci 13:336-
758 349.

759 Burns GA, Young MP (2000) Analysis of the connectional organization of neural systems associated
760 with the hippocampus in rats. Phil Trans R Soc B 355:55-70.

761 Chen BL, Hall DH, Chklovskii DB (2006) Wiring optimization can relate neuronal structure and
762 function. Proc Natl Acad Sci USA 103:4723-4728.

763 Chklovskii DB, Koulakov AA (2004) Maps in the brain: what can we learn from them? Annu Rev
764 Neurosci 27:369-392.

765 Chklovskii DB, Schikorski T, Stevens CF (2002) Wiring optimization in cortical circuits. Neuron 34:341-
766 347.

767 Colizza V, Flammini A, Serrano MA, Vespignani A (2006) Detecting rich-club ordering in complex
768 networks. Nat Phys 2:110-115.

769 Costa LD, Batista JL, Ascoli GA (2011) Communication structure of cortical networks. Front Comput
770 Neurosci 5:6.

771 DeFelipe J (2010) From the connectome to the synaptome: an epic love story. Science 330:1198-
772 1201.

773 Druckmann S, Feng L, Lee B, Yook C, Zhao T, Magee JC, Kim J (2014) Structured synaptic
774 connectivity between hippocampal regions. Neuron 81:629-640.

775 Erdős P, Rényi A (1960) On the evolution of random graphs. Publications of the Mathematical Institute
776 of the Hungarian Academy of Sciences 5:17-61.

777 Ewell LA, Jones MV (2010) Frequency-tuned distribution of inhibition in the dentate gyrus. J Neurosci
778 30:12597-12607.

779 Fagiolo G (2007) Clustering in complex directed networks. Phys Rev E Stat Nonlin Soft Matter Phys
780 76:026107.

781 Ferrante M, Migliore M, Ascoli GA (2009) Feed-forward inhibition as a buffer of the neuronal input-
782 output relation. Proc Natl Acad Sci USA 106:18004-19009.

783 Fu Y, Rusznák Z, Herculano-Houzel S, Watson C, Paxinos G (2013) Cellular composition
784 characterizing postnatal development and maturation of the mouse brain and spinal cord. Brain Struct
785 Func 218:1337-1354.

786 Fu Y, Kaneko M, Tang Y, Alvarez-Buylla A, Stryker MP (2015) A cortical disinhibitory circuit for
787 enhancing adult plasticity. Elife 4:e05558.

788 Gulyás AI, Hájos N, Freund TF (1996) Interneurons containing calretinin are specialized to control
789 other interneurons in the rat hippocampus. J Neurosci 16:3397-3411.

790 Gulyás AI, Megías M, Emri Z, Freund TF (1999) Total number and ratio of excitatory and inhibitory
791 synapses converging onto single interneurons of different types in the CA1 area of the rat
792 hippocampus. J Neurosci 19:10082-10097.

793 Guzman SJ, Schlögl A, Frotscher M, Jonas P (2016) Synaptic mechanisms of pattern completion in
794 the hippocampal CA3 network. Science 353:1117-1123.

795 Hamilton DJ, Wheeler DW, White CM, Rees CL, Komendantov AO, Bergamino M, Ascoli GA (2016)
796 Name-calling in the hippocampus (and beyond): coming to terms with neuron types and properties.
797 Brain Informatics (in press).

798 Harriger L, van den Heuvel MP, Sporns O (2012) Rich club organization of macaque cerebral cortex
799 and its role in network communication. PLOS ONE 7:e46497.

800 Hilgetag CC, Goulas A (2016) Is the brain really a small-world network?. Brain Struct Func 221:2361-
801 2366.

802 Hosseini-Sharifabad M, Nyengaard JR (2007) Design-based estimation of neuronal number and
803 individual neuronal volume in the rat hippocampus. J Neurosci Methods 162:206-214.

804 Insel TR, Landis SC, Collins FS (2013) The NIH brain initiative. Science 340:687-688.

805 Jiang X, Shen S, Cadwell CR, Berens P, Sinz F, Ecker AS, Patel S, Tolias AS (2015) Principles of
806 connectivity among morphologically defined cell types in adult neocortex. Science 350:aac9462.

807 Jones MW, McHugh TJ (2011) Updating hippocampal representations: CA2 joins the circuit. TINS
808 34:526-535.

809 Kasthuri N et al. (2015) Saturated reconstruction of a volume of neocortex. Cell 162:648-661.

Kasthuri N, Lichtman JW (2007) The rise of the 'projectome'. Nat Methods 4:307-308.

Klemm K, Eguiluz VM (2002) Growing scale-free networks with small-world behavior. Phys Rev E Stat Nonlin Soft Matter Phys 65:057102.

Krzywinski M, Schein J, Birol I, Connors J, Gascoyne R, Horsman D, Jones SJ, Marra MA (2009) Circos: an information aesthetic for comparative genomics. Genome Res 19:1639-1645.

Larimer P, Strowbridge BW (2008) Nonrandom local circuits in the dentate gyrus. J Neurosci 28: 12212-12223.

Latora V, Marchiori M (2001) Efficient behavior of small-world networks. Phys Rev E Stat Nonlin Soft Matter Phys 87:198701.

Lee S, Kruglikov I, Huang ZJ, Fishell G, Rudy B (2013) A disinhibitory circuit mediates motor integration in the somatosensory cortex. Nat Neurosci 16:1662-1670.

Leicht EA, Newman ME (2008) Community structure in directed networks. Phys Rev Lett 100:118703.

Letzkus JJ, Wolff SB, Meyer EM, Tovote P, Courtin J, Herry C, Lüthi A (2011) A disinhibitory microcircuit for associative fear learning in the auditory cortex. Nature 480:331-335.

Letzkus JJ, Wolff SB, Lüthi A (2015) Disinhibition, a circuit mechanism for associative learning and memory. Neuron 88:264-276.

Leuner B, Gould E (2010) Structural plasticity and hippocampal function. Annu Rev Psychol 61:111-140.

Lydersen S, Fagerland MW, Laake P (2009) Recommended tests for association in 2 × 2 tables. Stat Med 28:1159-1175.

Markram H et al. (2015) Reconstruction and simulation of neocortical microcircuitry. Cell 163:456-492.

831 McAuley JJ, da Fontoura Costa L, Caetano TS (2007) Rich-club phenomenon across complex
832 network hierarchies. Appl Phys Lett 91:084103.

833 Megías M, Emri ZS, Freund TF, Gulyás AI (2001) Total number and distribution of inhibitory and
834 excitatory synapses on hippocampal CA1 pyramidal cells. Neuroscience 102:527-540.

835 Milo R, Shen-Orr S, Itzkovitz S, Kashtan N, Chklovskii D, Alon U (2002) Network motifs: simple
836 building blocks of complex networks. Science 298:824-827.

837 Milo R, Itzkovitz S, Kashtan N, Levitt R, Shen-Orr S, Ayzenshtat I, Sheffer M, Alon U (2004)
838 Superfamilies of evolved and designed networks. Science 303:1538-1542.

839 Mishchenko Y, Hu T, Spacek J, Mendenhall J, Harris KM, Chklovskii DB (2010) Ultrastructural
840 analysis of hippocampal neuropil from the connectomics perspective. Neuron 67:1009-1020.

841 Mišić B, Sporns O, McIntosh AR (2014) Communication efficiency and congestion of signal traffic in
842 large-scale brain networks. PLoS Comput Biol 10:e1003427.

843 Mitra PP (2014) The circuit architecture of whole brains at the mesoscopic scale. Neuron 83:1273-
844 1283.

845 Nassar M, Simonnet J, Lofredi R, Cohen I, Savary E, Yanagawa Y, Miles R, Fricker D (2014) Diversity
846 and overlap of parvalbumin and somatostatin expressing interneurons in mouse presubiculum. Front
847 Neural Circuits 9:20.

848 Newman ME (2004) Fast algorithm for detecting community structure in networks. Phys Rev E Stat
849 Nonlin Soft Matter Phys 69:066133.

850 Nitz D, McNaughton B (2004) Differential modulation of CA1 and dentate gyrus interneurons during
851 exploration of novel environments. J Neurophysiol 91:863-872.

852 Oh SW et al. (2014) A mesoscale connectome of the mouse brain. Nature 508:207-214.

853 Pearson K (1905) Das Fehlergesetz und Seine Verallgemeinerungen Durch Fechner und Pearson. A
854 Rejoinder. Biometrika. 4:169-212.

855 Pi HJ, Hangya B, Kvitsiani D, Sanders JI, Huang ZJ, Kepecs A (2013) Cortical interneurons that
856 specialize in disinhibitory control. Nature 503:521-524.

857 Prettejohn B, Berryman M, McDonnell M (2011) Methods for generating complex networks with
858 selected structural properties for simulations: a review and tutorial for neuroscientists. Front Comput
859 Neurosci 5:11.

860 Rubinov M, Sporns O (2010) Complex network measures of brain connectivity: uses and
861 interpretations. Neuroimage 52:1059-1069.

862 Santana R, Bielza C, Larrañaga P (2011) Optimizing brain networks topologies using multi-objective
863 evolutionary computation. Neuroinformatics 9:3-19.

864 Shanahan M, Bingman VP, Shimizu T, Wild M, Güntürkün O (2013) Large-scale network organization
865 in the avian forebrain: a connectivity matrix and theoretical analysis. Front Comput Neurosci 7:89.

866 Shen-Orr SS, Milo R, Mangan S, Alon U (2002) Network motifs in the transcriptional regulation
867 network of Escherichia coli. Nat Genet 31:64-68.

868 Shepherd GM (1991) Foundations of the neuron doctrine. New York: Oxford UP.

869 Shih CT, Sporns O, Yuan SL, Su TS, Lin YJ, Chuang CC, Wang TY, Lo CC, Greenspan RJ, Chiang
870 AS (2015) Connectomics-based analysis of information flow in the Drosophila brain. Curr Biol
871 25:1249-1258.

872 Song S, Sjöström PJ, Reigl M, Nelson S, Chklovskii DB (2005) Highly nonrandom features of synaptic
873 connectivity in local cortical circuits. PLoS Biol 3:e68.

874 Sporns O, Tononi G, Edelman GM (2000) Theoretical neuroanatomy: relating anatomical and
875 functional connectivity in graphs and cortical connection matrices. Cereb Cortex 10:127–141.

876 Sporns O, Kötter R (2004) Motifs in brain networks. PLoS Biol 2:e369.

877 Sporns O, Tononi G, Kötter R (2005) The human connectome: a structural description of the human
878 brain. PLoS Comput Biol 1:e42.

879 Sridharan D, Knudsen EI (2015) Selective disinhibition: A unified neural mechanism for predictive and
880 post hoc attentional selection. Vision Res 116:194-209.

881 Storey JD (2002) A direct approach to false discovery rates. J R Stat Soc: Series B (Statistical
882 Methodology) 64:479-498.

883 Tateno K, Hayashi H, Ishizuka S (2007) Synchronized spike selection in a hippocampal dentate gyrus
884 network model in the theta frequency range. International Congress Series 1301:79-82.

885 Timme NM, Ito S, Myroshnychenko M, Nigam S, Shimono M, Yeh FC, Hottowy P, Litke AM, Beggs JM
886 (2016) High-Degree Neurons Feed Cortical Computations. PLoS Comput Biol 12:e1004858.

887 van den Heuvel MP, Sporns O (2011) Rich-club organization of the human connectome. J Neurosci
888 31:15775-15786.

889 van den Heuvel MP, Sporns O (2013) Network hubs in the human brain. Trends Cogn Sci 17:683-696.

890 Van Essen DC, Smith SM, Barch DM, Behrens TE, Yacoub E, Ugurbil K, WU-Minn HCP Consortium
891 (2013) The WU-Minn human connectome project: an overview. Neuroimage 80:62-79.

892 van Strien NM, Cappaert NL, Witter MP (2009) The anatomy of memory: an interactive overview of
893 the parahippocampal-hippocampal network. Nat Rev Neurosci 10:272-282.

894 Vida I, Frotscher M (2000) A hippocampal interneuron associated with the mossy fiber system. Proc
895 Natl Acad Sci USA 97:1275-1280.

896 Vogels TP, Abbott LF (2009) Gating multiple signals through detailed balance of excitation and
897 inhibition in spiking networks. Nature Neurosci 12:483-491.

898 Watts DJ, Strogatz SH (1998) Collective dynamics of 'small-world' networks. Nature 393:440-442.

899 West MJ, Slomianka LH, Gundersen HJ (1991) Unbiased stereological estimation of the total number
900 of neurons in the subdivisions of the rat hippocampus using the optical fractionator. Anat Rec
901 231:482-497.

902 Westfall PH (2014) Kurtosis as peakedness, 1905-2014. RIP. Am Stat 68:191-195.

903 Westfall PH, Young SS (1993) Resampling-based multiple testing: Examples and methods for p-value
904 adjustment. New York: John Wiley & Sons.

905 Wheeler DW, White CM, Rees CL, Komendantov AO, Hamilton DJ, Ascoli GA (2015)
906 Hippocampome.org: a knowledge base of neuron types in the rodent hippocampus. Elife 4:e09960.

907 Wig GS, Schlaggar BL, Petersen SE (2011) Concepts and principles in the analysis of brain networks.
908 Ann N Y Acad Sci 1224:126-146.

909 Woodson W, Nitecka L, Ben-Ari Y (1989) Organization of the GABAergic system in the rat
910 hippocampal formation: a quantitative immunocytochemical study. J Comp Neurol 280:254-271.

911 Yizhar O, Fenno LE, Prigge M, Schneider F, Davidson TJ, O'Shea DJ, Sohal VS, Goshen I,
912 Finkelstein J, Paz JT, Stehfest K (2011) Neocortical excitation/inhibition balance in information
913 processing and social dysfunction. Nature 477:171-178.

914 Zaslaver A, Mayo AE, Rosenberg R, Bashkin P, Sberro H, Tsalyuk M, Surette MG, Alon U (2004)
915 Just-in-time transcription program in metabolic pathways. Nat Genet 36:486-491.

916 Zhang S, Xu M, Kamigaki T, Do JP, Chang WC, Jenvay S, Miyamichi K, Luo L, Dan Y (2014) Long-
917 range and local circuits for top-down modulation of visual cortex processing. Science 345:660-665.

918 Zhou S, Mondragón RJ (2004) The rich-club phenomenon in the Internet topology. IEEE Commun Lett
919 8:180-182.

Zingg B, Hintiryan H, Gou L, Song MY, Bay M, Bienkowski MS, Foster NN, Yamashita S, Bowman I, Toga AW, Dong HW (2014). Neural networks of the mouse neocortex. Cell 156:1096-1111.

Legends

Table 1. Neuron type glossary: 122 types ordered first by sub-region, then by primary neurotransmitter, then alphabetically. Asterisks indicate types that are either not well known or contain relatively little molecular marker and electrophysiological evidence.

Figure 1. Potential connectivity of neuron types. (A) Partial matrix showing axonal and dendritic locations for selected DG, CA3, and CA2 types within certain parcels of the hippocampal formation (full matrix available online at Hippocampome.org/morphology). Type names in bold are glutamatergic and in gray are GABAergic. Red boxes with horizontal lines correspond to axons; blue with vertical lines to dendrites; purple with horizontal and vertical lines to both axons and dendrites; black circles indicate soma location(s). Potential connections of Granule cells are spotlighted with red arrows. Parcel abbreviations for DG: SMo, outer stratum moleculare; SMi, inner stratum moleculare; SG, stratum granulosum; H, hilus; for CA3/CA2: SLM, stratum lacunosum-moleculare; SR, stratum radiatum; SL, stratum lucidum; SP, stratum pyramidale; SO, stratum oriens. (B) Representative illustration of the overlapping spatial distributon (indicative of potential connectivity) of Granule cell axons (right) and MFA ORDEN cell dendrites (left) in CA3 SL and SP (for both neurons: axons in red; dendrites in black). Morphological reconstruction of the granule cell downloaded from NeuroMorpho.Org (Ascoli et al., 2007), with layers drawn in, from a tracing originally presented in Bausch et al. (2006). Permission to reprint the MFA ORDEN cell (Vida and Frotscher, 2000) granted by PNAS (Copyright 2000 National Academy of Sciences, U.S.A.). (C) Screenshot from the novel online toolbox (Hippocampome.org/connectivity) illustrating all information potentially received (arrows in) and sent (arrows out) by Granule cells (black connections excitatory; orange inhibitory).

945

946 **Figure 2**. Comparison of the HC to well-known types of equivalently sized random networks. (A)
947 Broad categorizations, indicated by background shading from the four corners, aid in grouping and
948 analyzing network topology along two dimensions of interest: CC and CPL. Data points for six types of
949 random networks are averaged from 1,000-network datasets; standard deviations are illustrated by
950 the diameter. (B) The combination of high CC and low CPL in the HC results in an optimally low
951 overall communication cost in the network. BA=Barabási-Albert, ER=Erdős-Rényi, KE=Klemm-
952 Eguílez, Latt=square lattice, WS=Watts-Strogatz.

953

954 **Figure 3**. Modular structure of the potential hippocampal connectome. (A) Chord diagram of the
955 potential connectivity among all 122 types (produced with Circos software: Krzywinski et al., 2009).
956 Thick chords with arrows emphasize the trisynaptic loop (perforant pathway lines: dark green;
957 temporoammonic path: light green; mossy fibers: red; Schaffer collaterals: blue; projection from CA1
958 to EC layer V: orange); other connections are colored randomly to optimize visibility. Types are
959 identifiable both by numbers in brackets (names provided in Table 1) and axon-dendrite patterning
960 within the sub-region of their soma location (colored box convention and layer ordering from inside-out
961 as in Fig. 1; layers for CA1: SLM, SR, SP, SO; for subiculum: stratum moleculare, SP, polymorphic
962 layer; for EC: I-VI). Shaded bars in the innermost ring show the total number of (signed) connections
963 made by that type; excitatory types have outward-facing black bars and inhibitory types inward-facing
964 gray bars. (B) Modularity scores (Q) for the entire network and for the four detected modules. (C) The
965 communities correspond closely to the DG (module connection density=75.9%), CA3 (59.3%), CA1
966 (64.6%), and EC (70.1%; not shown). Numbered types and colored arrows as in panel A.

967

968 **Figure 4**. Breakdown of degree distribution to isolate neuron types with unusual connectivity. (A) The
969 difference in the axonal and dendritic architecture is evident in the OD (red data series) and ID (blue)

970 distributions. (B) The two OD tails are respectively attributable to highly connected hubs within the
971 subset of neuron types that project to another sub-region (green series; positive skewness) and to
972 certain local neuron types with highly specific connectivity (gray; negative skewness).

973

974 **Table 2**. Identification of hubs and anti-hubs with high and low TD, respectively. Polarities quantify the
975 net in/out balance of information flow. Type names in black are excitatory; gray inhibitory.

976

977 **Figure 5**. Nested rich clubs within the HC. (A) Top: distribution of nodes by TD. Bottom: nodes with
978 TD≥55 are members of a densely interconnected rich club. Eight members of this club are also
979 members of a second "ultra-rich" club level (dark purple shading; light purple shading indicates
980 members of RC I but not RC II). (B) Connection densities of RC I and RC II are elevated compared to
981 the rest of the network. (C) Modular analysis of each RC tier. (D) The 56 neuron types of RC I (top)
982 and the subset constituting RC II (bottom).

983

984 **Figure 6**. Alternate pathways between nodes afford resilience to the network. (A) Length of the
985 shortest directed route between each pair of neuron types. Pre-synaptic types are in rows, post-
986 synaptic types in columns; see Table 1 for type names and ordering. Color gradient key: yellow=direct
987 connection; orange, red, and dark red indicate 2, 3, and 4 steps, respectively; black=highest path
988 length (5 steps). (B) Orange labels indicate the percentage of type pairs that can be bridged by a path
989 of a given length, k (shown for k≤5). In addition, at each k, blue columns show the average number of
990 available conduits across all pairs of types. (C) For k=2, peak height in a three-dimensional plot
991 indicates the number of two-step paths between types. (D) Absorption measures the average length of
992 all routes from (rows) and to (columns) other types. (E) Driftness is relatively low for most type pairs,
993 pointing to the availability of multiple pathways between nodes that are similar in length to the shortest
994 path. Color gradient for D and E as in A.

Figure 7. Superpatterns and HC usage. (A) Connectivity superpattern trimers are unweighted subgraphs of three nodes (disconnected superpatterns outlined in gray). (B) Counts of disconnected and connected superpatterns. (C) Percentage of connected superpatterns localized to a given module or found between modules. (D) Within CA1, superpattern usage also varies by cell type, as indicated by ratios of pyramidal cells to interneurons (blue line) and perisomatic interneurons to dendritic-targeting neurons (dotted red line).

Figure 8. Weighted trimers analysis based on excitatory/inhibitory neuron type distinction. (A) The 8 patterns that constitute superpattern F, the single uplinked mutual dyad. Black lines and nodes are excitatory, gray lines and nodes are inhibitory, blue lines indicate reciprocal connections that are excitatory in one direction and inhibitory in the other. ES values are shown in boxes where background shading indicates strongly and mildly excitatory and inhibitory patterns; key shown in B. (B) Relative importance of each ES to the DG, CA3, and CA1 modules. (C) Pattern F4 is heavily employed by CA3 and CA3c Pyramidal cells; relatively light usage of this pattern by CA1 Pyramidal cells and CA3 interneurons is shown for comparison. (D) The CA3 Pyramidal cell connected pattern fingerprint (brown) is plotted on top of the overall HC fingerprint (light blue) using a logarithmic scale.

Figure 9. Three-node feedback loops (superpattern G) are generally avoided in HC in favor of other 2-step chains, such as feedforward loops (superpattern E). The excitatory/inhibitory combinations of these patterns are displayed in the right and left columns along with representative neuron type groupings and a computational interpretation. Black dots and arrows indicate excitatory types and connections; gray signifies inhibitory types and connections; blue dots, located at the output of the loop, are excitatory in one pattern combination and inhibitory in the other. Total network occurrences for each pattern are shown in square brackets.

Figure 10. (A) Motifs and anti-motifs are largely determined by HC superpattern topology. While some superpatterns are neutral, most superpatterns are strong motifs. Only superpatterns D, G, and I are severely underutilized relative to the population of random networks. (B-D) The motif/anti-motif balance of individual superpatterns in the network does not necessarily hold for individual modules (e.g. superpatterns C and J).

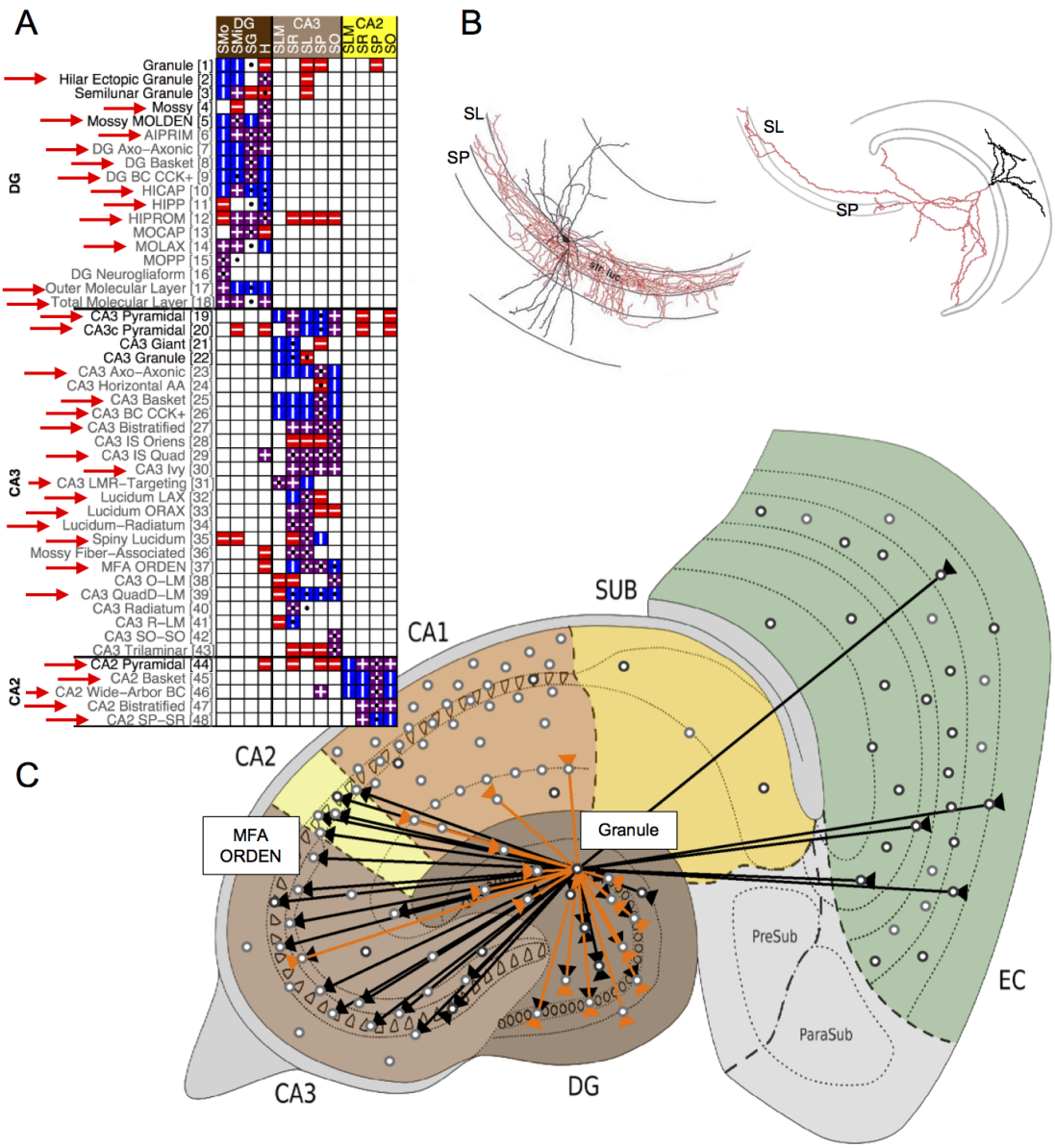

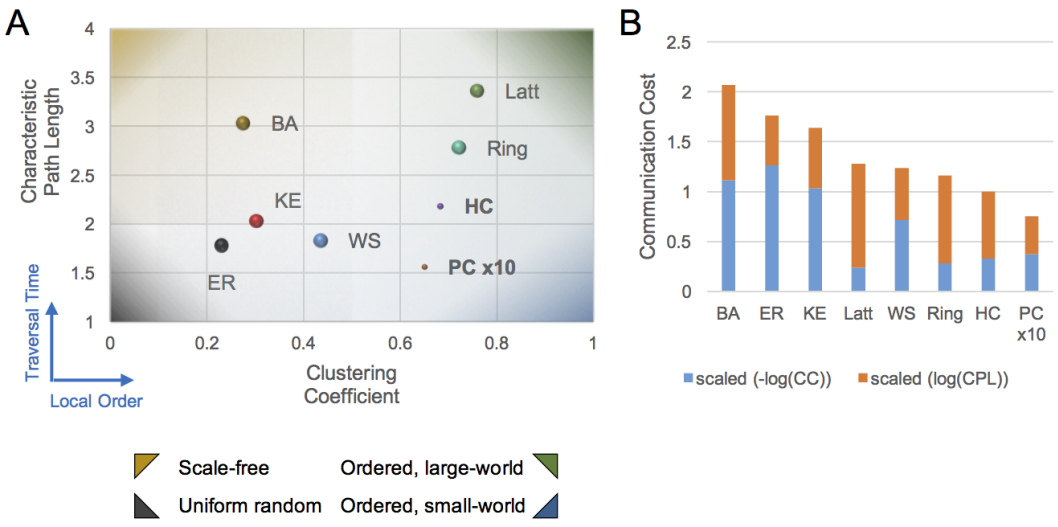

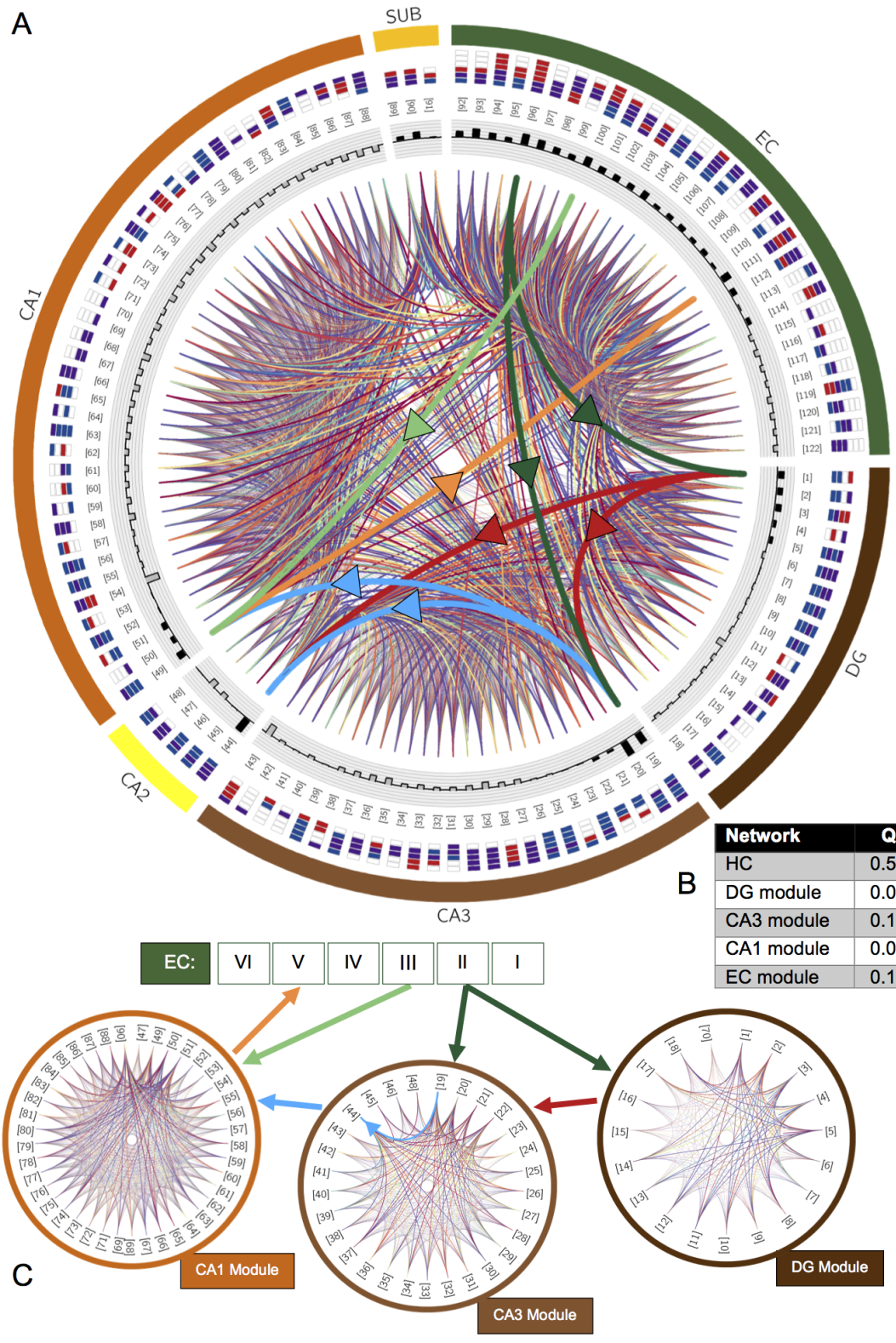

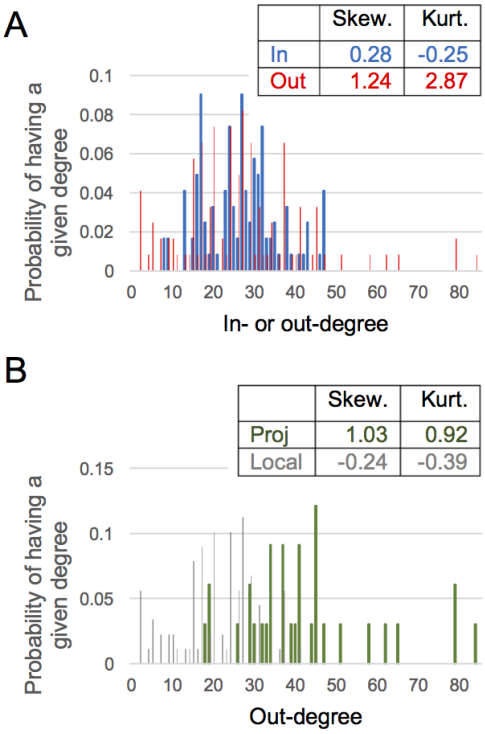

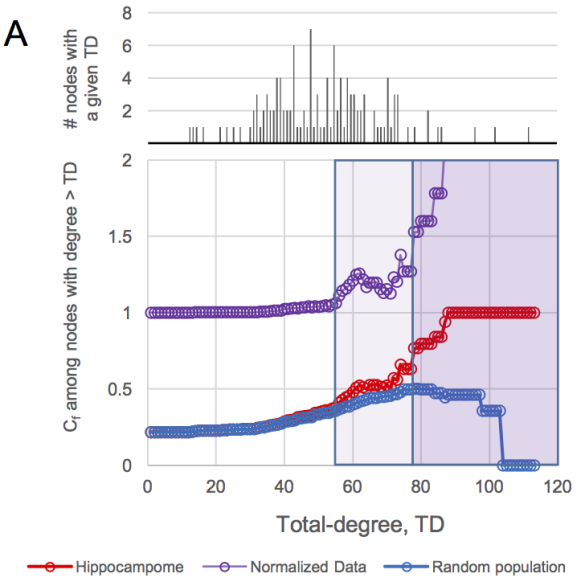

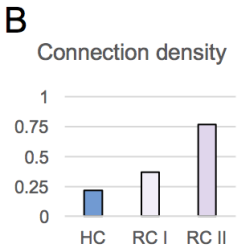

C

	RC I	RC II	Nodes
HC	56	8	122
DG	5	0	19
CA3	9	3	29
CA1	27	5	41
EC	15	0	33

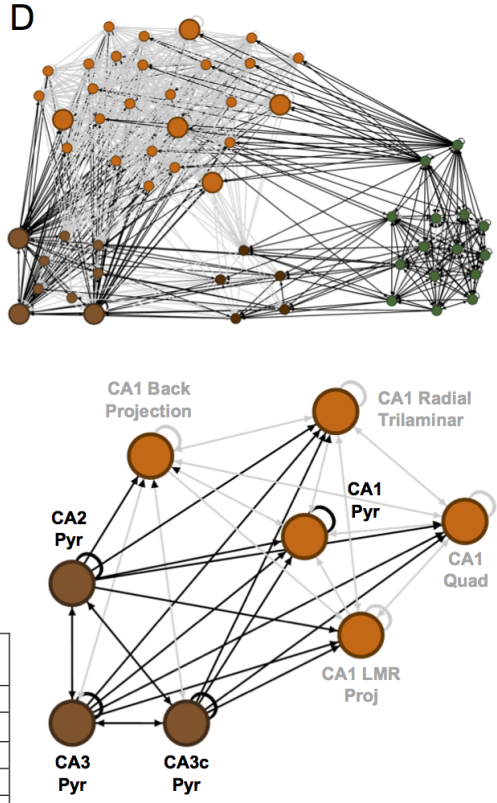

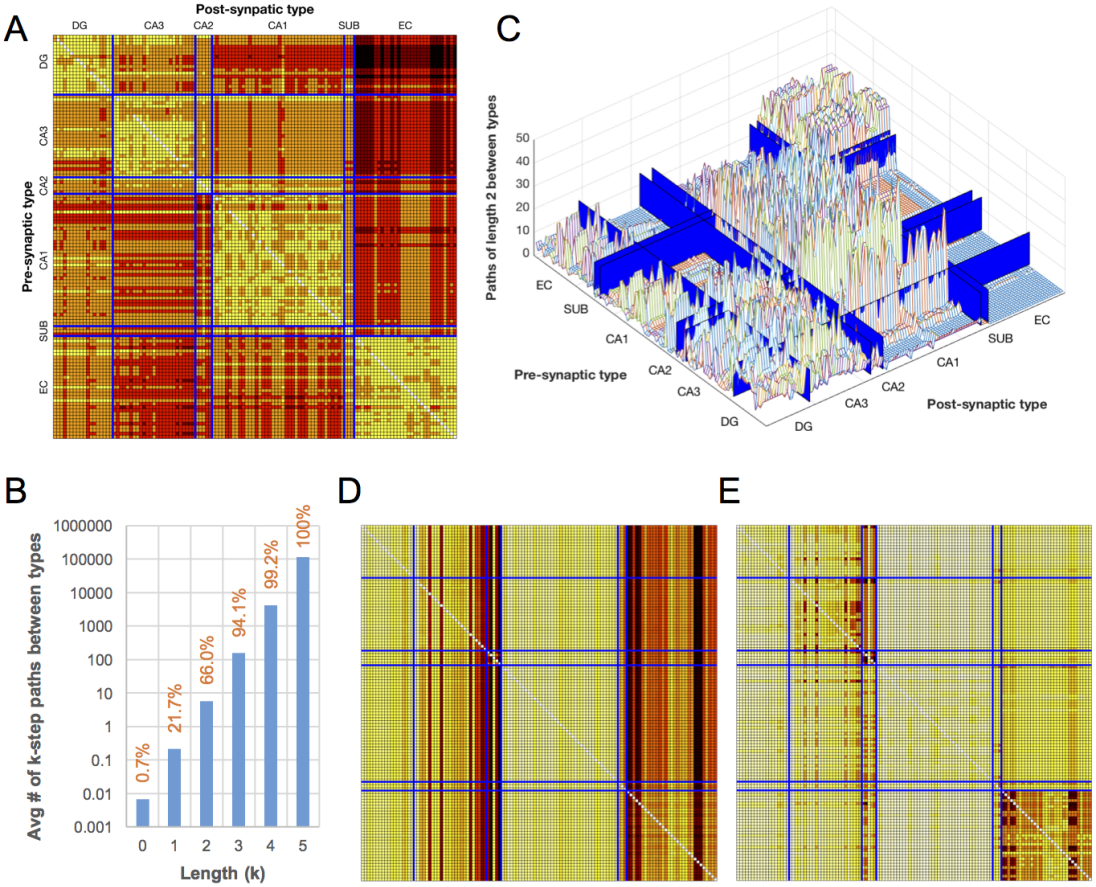

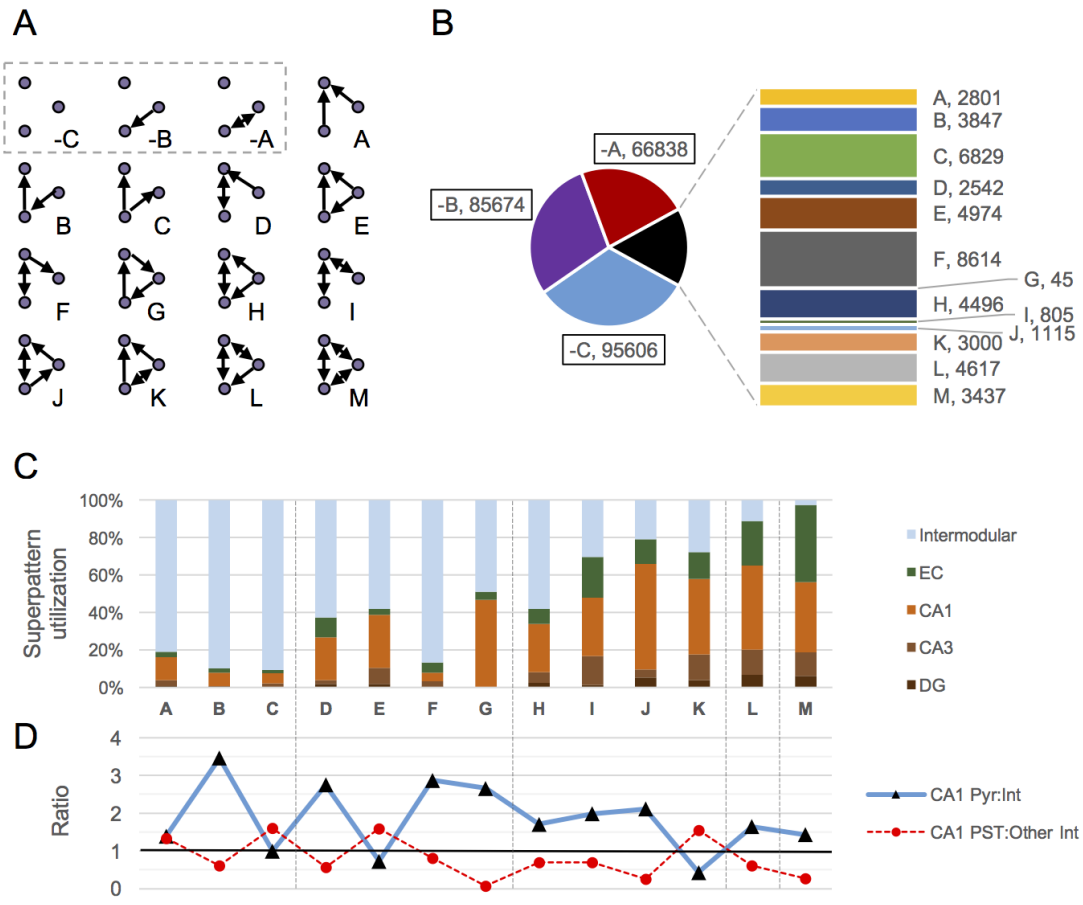

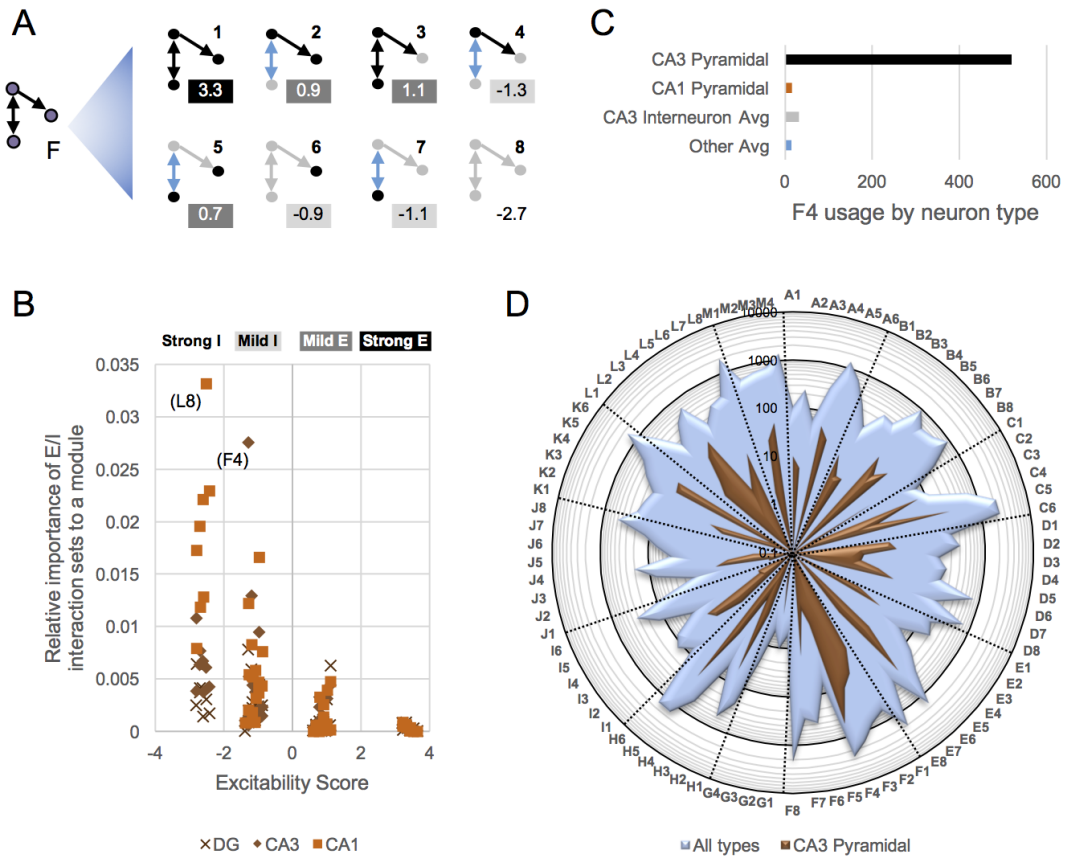

Pattern and examples	Interpretation	Pattern and examples	Interpretation
E1 [167] & E5 [352] 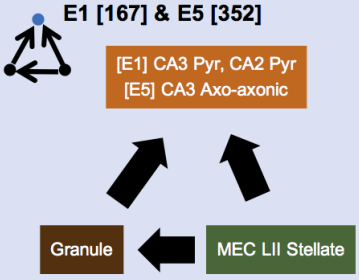	Feed-forward excitation as part of the perforant path shortcuts DG onto many CA3 module excitatory [E1] and inhibitory [E5] types	**G1 [6]** 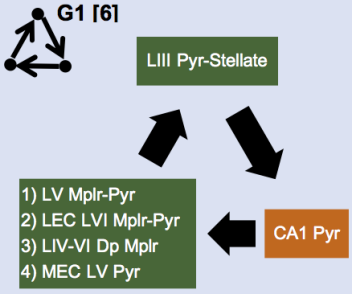	Excitatory feedback involving the TA pathway; loop goes from deep to superficial EC and to CA1, before returning
E2 [215] & E6 [1661] 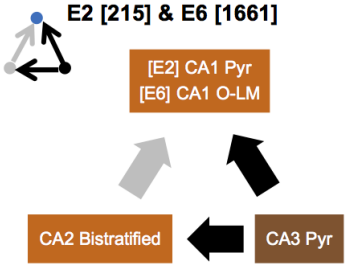	Classical feed-forward inhibition originating from CA3 Pyr on excitatory [E2] and inhibitory [E6] types in CA1. E2 also used by perforant path in DG.	**G2 [11]** 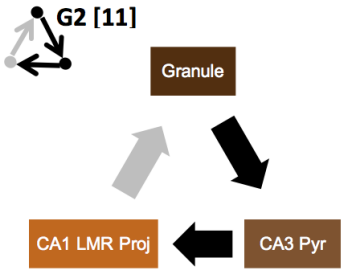	Feedback inhibition provided to propagating TSL signals by projecting inhibitory cells
E3 [57] & E7 [279] 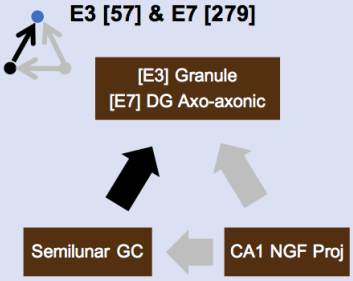	Parallel direct and indirect (via dampening) inhibition on excitatory [E3] and inhibitory [E7] types.	**G3 [5]** 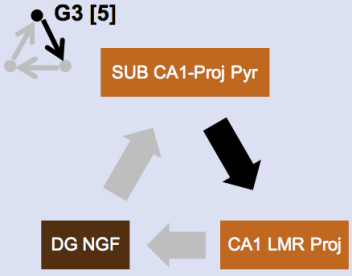	Two inhibitory types in a feedback loop with an excitatory type
E4 [155] & E8 [2088] 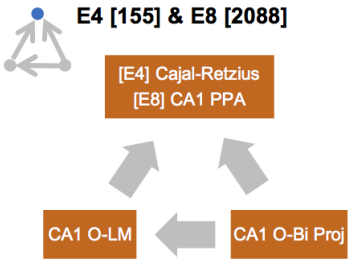	Feedforward loops with 2 interneurons terminating on an excitatory type [E4] are relatively rare compared to similar loops terminating on inhibitory types [E8].	**G4 [23]** 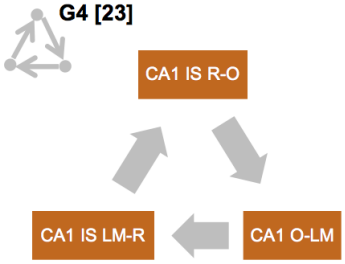	Inhibitory feedback cycle, usually involving at least one CA1 interneuron-specific type (20/21 occurrences)

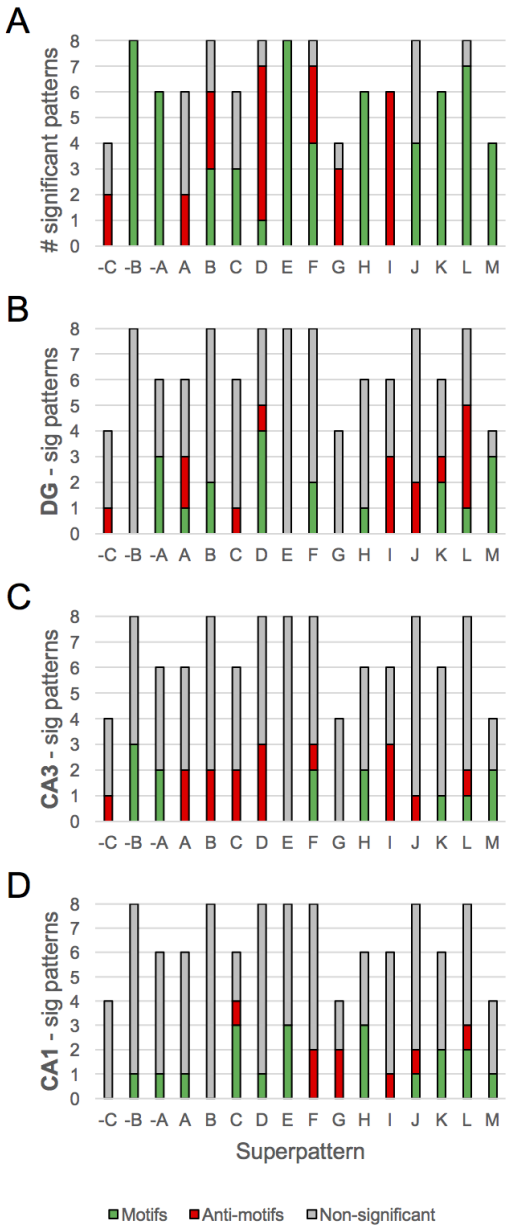

[1] Granule	[41] CA3 R-LM	[82] CA1 R-Recv Apical-Targeting *
[2] Hilar Ectopic Granule *	[42] CA3 SO-SO (oriens-oriens) *	[83] Schaffer Collateral-Associated
[3] Semilunar Granule	[43] CA3 Trilaminar	[84] SCR R-Targeting *
[4] Mossy	[44] CA2 Pyramidal	[85] CA1 SO-SO (oriens-oriens)
[5] Mossy MOLDEN *	[45] CA2 Basket	[86] CA1 Hipp-Subiculum Proj ENK+ *
[6] AIPRIM (Aspiny int w/ proj. to SMi)	[46] CA2 Wide-Arbor Basket	[87] CA1 Trilaminar
[7] DG Axo-Axonic	[47] CA2 Bistratified	[88] CA1 Radial Trilaminar
[8] DG Basket	[48] CA2 SP-SR	[89] SUB EC-Projecting Pyramidal
[9] DG Basket CCK+	[49] CA1 Pyramidal	[90] SUB CA1-Projecting Pyramidal
[10] HICAP	[50] Cajal-Retzius	[91] SUB Axo-axonic
[11] HIPP	[51] CA1 Radiatum Giant	[92] LI-II Multipolar-Pyramidal
[12] HIPROM (Hilar int w/ proj. to SMo)	[52] CA1 Axo-Axonic	[93] LI-II Pyramidal-Fan
[13] MOCAP (Molecular Commissural-Associational Pathway related) *	[53] CA1 Horizontal Axo-Axonic	[94] MEC LII Pyramidal-Multiform
	[54] CA1 Back-Projection	[95] MEC LII Oblique Pyramidal *
[14] MOLAX	[55] CA1 Basket	[96] MEC LII Stellate
[15] MOPP	[56] CA1 Basket CCK+	[97] LII-III Pyramidal-Tripolar
[16] DG Neurogliaform	[57] CA1 Horizontal Basket	[98] LEC LIII Multipolar Principal *
[17] Outer Molecular Layer *	[58] CA1 Bistratified	[99] MEC LIII Multipolar Principal *
[18] Total Molecular Layer	[59] CA1 Int-specific LMO-O *	[100] LIII Pyramidal
[19] CA3 Pyramidal	[60] CA1 Int-specific LM-R	[101] LEC LIII Complex Pyramidal *
[20] CA3c Pyramidal	[61] CA1 Int-specific LMR-R	[102] MEC LIII Complex Pyramidal *
[21] CA3 Giant	[62] CA1 Int-specific O-R *	[103] MEC LIII Bipolar Complex Pyr
[22] CA3 Granule	[63] CA1 Int-spec O-Target QuadD	[104] LIII Pyramidal-Stellate
[23] CA3 Axo-Axonic	[64] CA1 Int-specific R-O *	[105] LIII Stellate
[24] CA3 Horizontal Axo-Axonic *	[65] CA1 Int-specific RO-O *	[106] LIII-V Bipolar Pyramidal
[25] CA3 Basket	[66] CA1 Ivy	[107] LIV-V Pyramidal-Horizontal
[26] CA3 Basket CCK+	[67] CA1 LMR	[108] LIV-VI Deep Multipolar
[27] CA3 Bistratified	[68] CA1 LMR Projecting	[109] MEC LV Multipolar-Pyramidal
[28] CA3 Interneuron-specific Oriens *	[69] CA1 Neurogliaform	[110] LV Deep Pyramidal
[29] CA3 Interneuron-specific Quad *	[70] CA1 Neurogliaform Projecting	[111] MEC LV Pyramidal
[30] CA3 Ivy	[71] CA1 O-LM	[112] MEC LV Superficial Pyramidal
[31] CA3 LMR-Targeting	[72] CA1 Recurrent O-LM	[113] MEC LV-VI Pyr-Polymorph
[32] Lucidum LAX (lucidum axons) *	[73] CA1 O-LMR	[114] LEC LVI Multipolar-Pyramidal *
[33] Lucidum ORAX (oriens axons)	[74] CA1 Oriens/Alveus	[115] LII Axo-Axonic
[34] Lucidum-Radiatum *	[75] CA1 Oriens-Bistratified	[116] MEC LII Basket
[35] Spiny Lucidum	[76] CA1 O-Bistrat Projecting *	[117] LII Basket-Multipolar Int
[36] Mossy Fiber-Associated (MFA)	[77] CA1 OR-LM *	[118] LEC LIII Multipolar Int
[37] MFA ORDEN (oriens-dendrites)	[78] CA1 Perforant Path-Associated	[119] MEC LIII Multipolar Int
[38] CA3 O-LM	[79] CA1 Perforant Path QuadD	[120] MEC LIII Superficial Multiplr Int
[39] CA3 QuadD-LM	[80] CA1 Quadrilaminar	[121] LIII Pyramidal-Looking Int
[40] CA3 Radiatum *	[81] CA1 Radiatum	[122] MEC LIII Superficial Trilayer Int

	Module	Neuron type	Out-deg	In-deg	Total-deg	Polarity
Global hubs	CA3	CA3c Pyramidal	84	30	114	-0.47
	CA1	CA1 Back-Projection	79	25	104	-0.52
	CA3	CA3 Pyramidal	65	33	98	-0.33
	CA3	CA2 Pyramidal	79	9	88	-0.80
	CA1	CA1 Pyramidal	41	46	87	0.06
	CA1	CA1 Quadrilaminar	41	43	84	0.02
	CA1	CA1 Radial Trilaminar	37	47	84	0.12
	CA1	CA1 LMR Projecting	45	35	80	-0.13
	EC	MEC LV Pyramidal	51	27	78	-0.31
	CA3	CA3 Trilaminar	62	13	75	-0.65
Global anti-hubs	CA1	SUB Axo-axonic	2	15	17	0.76
	CA3	CA3 Horizontal AA	2	13	15	0.73
	CA3	CA2 Basket	5	9	14	0.29
	CA3	CA2 SP-SR	5	8	13	0.23
Provincial hubs	DG	MOLAX	17	32	49	0.31
	CA3	CA3 Bistratified	26	28	54	0.04
	CA3	CA3 Ivy	26	25	51	-0.02
	CA1	CA1 Oriens-Bistratified	36	24	60	-0.20